2015-01-01

Elucidating the Electronic Structure of Multiple Bonded Systems: SynThesis and Characterization of Bimetallic Tungsten and Ruthenium Complexes

Karen Ventura
University of Texas at El Paso, kventura@miners.utep.edu

ELUCIDATING THE ELECTRONIC STRUCTURE OF MULTIPLE BONDED SYSTEMS:

SYNTHESIS AND CHARACTERIZATION OF BIMETALLIC

TUNGSTEN AND RUTHENIUM COMPLEXES.

KAREN VENTURA,

Department of Chemistry

APPROVED:

Dino Villagrán, Ph.D, Chair

Keith H. Pannell, Ph.D

Skye Fortier, Ph.D

Cristian Botez, Ph.D

Charles Ambler, Ph.D.
Dean of the Graduate School

Dedication

To my parents, Martin and Sandra, my siblings Arnoldo and Ximena, and God, because family is where our journey begins.

ELUCIDATING THE ELECTRONIC STRUCTURE OF MULTIPLE BONDED SYSTEMS: SYNTHESIS AND CHARACTERIZATION OF BIMETALLIC TUNGSTEN AND RUTHENIUM COMPLEXES

by

KAREN VENTURA, B.S.

THESIS

Presented to the Faculty of the Graduate School of

The University of Texas at El Paso

in Partial Fulfillment

of the Requirements

for the Degree of

MASTER OF SCIENCE

Department of Chemistry

THE UNIVERSITY OF TEXAS AT EL PASO

August 2015

Acknowledgements

First and foremost, I would like to thank my research advisor, Dr. Villagrán, for all of his support and guidance in my research and for his knowledge, enthusiasm, and immense patience.

In addition to my advisor, I would like to thank the members of my committee, Dr. Pannell, Dr. Fortier and Dr. Botez for their constructive commentary and their reliable advice. Additionally, I would like to thank Dr. Metta for his assistance in X-ray crystallography

I thank my fellow lab mates of the Villagrán lab, Nathalie, José, Yanyu, Mark and Nancy, for all of the chemistry discussions, sleepless nights before deadlines, for the drama, and for all the fun that we had together throughout these two years. I would also like to show gratitude to my undergraduate assistants Jacob, Luis, and Ivan for all of their hard work and for all the laughs we shared together, they made a lot of this research possible.

Special thanks to Cecilio, Jorge and Quang because everyone needs a team to rely on, to trust, and to open up to, also every now and then an organic chemist comes in handy.

Finally I would like to thank all the faculty and staff from the UTEP chemistry department, especially Dr. Narayan and Dr. Michael for their valuable advice and support in my graduate studies.

Abstract

The following study is presented in two sections. In the first section variable-temperature magnetic and structural data of two pairs of diruthenium isomers (having an idealized D_{4h} symmetry), one pair having axial ligands and the formula $Ru_2(DArF)_4Cl$ (where DArF is the anion of a diarylformamidine isomer, and Ar = *p*-anisyl or *m*-anisyl) and the other one being essentially identical but devoid of axial ligands and having the formula $[Ru_2(DArF)_4]BF_4$, show that the axial ligands have a significant effect on the electronic structure of the diruthenium core. Variable-temperature crystallographic and magnetic data as well as density functional theory (DFT) calculations unequivocally demonstrate the occurrence of π interactions between the p orbitals of the chlorine ligand and the π* orbitals in the Ru_2^{5+} cores. Electron paramagnetic resonance data show unambiguously that the unpaired electrons are in metal-based molecular orbitals.

On the second section a triple bonded compound $W_2(TPG)_2Cl_4$, with a D_{2h} symmetry at the core (where TPG is the anion of *N,N',N''*- triphenylguanidine), was synthesized and structurally characterized by single-crystal x-ray crystallography, FT-IR, NMR and Raman spectroscopies, and electrochemical methods. The W–W distance in the solid state is 2.2612(4) Å, and the compound shows two one-electron reversible reductions at ($E_{1/2}$) –0.73, and –1.04 V (vs Fc/Fc^+). A one-electron reduction of the compound resulted in a complex with a bond order of 3.5, which was characterized by Raman and EPR spectroscopies (g = 1.83). The Raman shift of the W–W bond of both complexes are, 290, and 315 cm^{-1}, respectively, consistent to the increase in bond order. DFT calculations were performed to aid in the assignment of the Raman shifts, and to help understand their electronic properties.

Table of Contents

List of Tables

List of Figures

List of Illustrations

Chapter 1: Introduction

An explosive growth in the study of metal-metal bonding was initiated by the discovery of a quadruple bond in $Re_2Cl_8^{2-}$ (Figure 1.1), more than 50 years ago.[1] The molecule consists of two rhenium atoms with a bond distance of ca. 2.50 Å, each metal bonded to four chlorine atoms in an eclipsed arrangement, resulting in D_{4h} symmetry. This configuration was rationalized as being due to the existence of a delta bond formed by lateral overlap of the corresponding *d* orbitals with *x* and *y* components. This finding marked the beginning of the understanding of new chemical possibilities that a delta bond could bring. Since then hundreds of compounds featuring high bond orders have been successfully synthesized and characterized. [1,54,55]

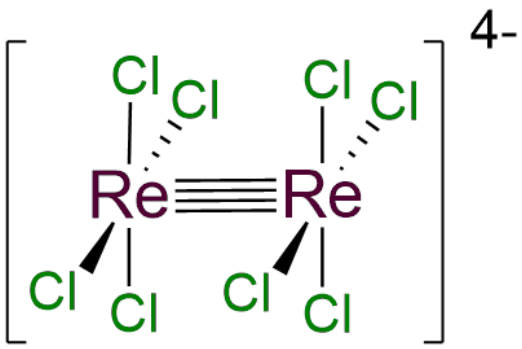

Figure 1.1. Quadruple bonded $Re_2Cl_8^{2-}$ anion, depicting a D_{4h} symmetry

This discovery also triggered the understanding of the nature of the metal-metal bond present in different configurations. For a general paddlewheel conformation, an idealized D_{4h} symmetry is used to describe the essence of the metal bonds. As depicted in Figure 1.2 the interaction between d_{z^2}– d_{z^2} orbitals from each metal give rise to a σ bond, while the overlap between d orbitals containing a z component (d_{zy} and d_{zx}) from each metal constitute both π bonds. The fourth bond, that is the δ bond, arises from the overlay of the d_{yx} orbitals from each

metal center. It is important to notice that the $d_{x^2-y^2}$ orbital in this symmetry is used for metal-ligand bonding, resulting in a maximum bond order of four.

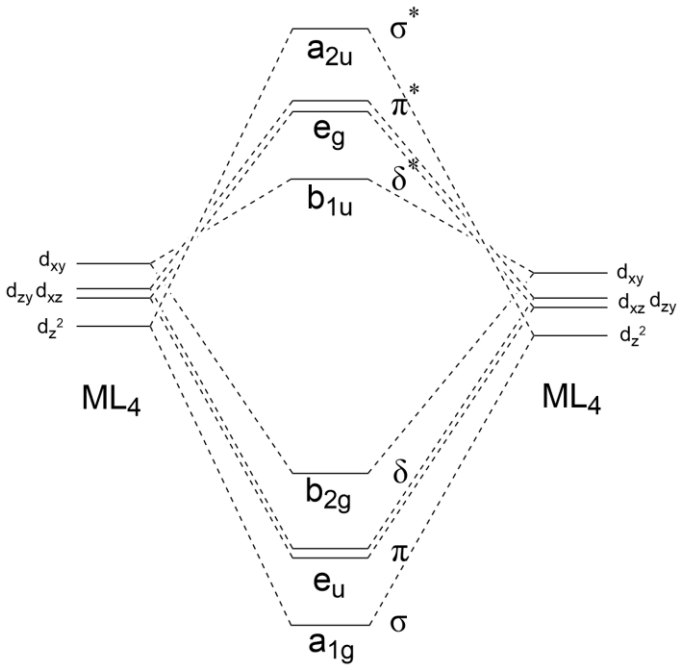

Figure 1.2. Idealized electronic structure for a M_2L_4 compound in a D_{4h} conformation.

A different electronic structure is elucidated for those compounds containing D_{2h} symmetry. Figure 1.3 illustrates the electronic configuration of a M_2L_2 compound. Comparable to that of the previously mentioned D_{4h} symmetry, the σ bond arises from the d_{z^2} overlap and the π bond originates from the overlay of the d_{zy} and d_{zx} components from each metal center, and finally a delta bond coming from the interaction of the d_{xy} orbitals is formed. Unlike the D_{4h} symmetry, the D_{2h} configuration can access the $d_{x^2-y^2}$ orbital for metal-metal bonding, since a lower number of ligands is used, lowering the contribution of the metal d orbitals in σ and π bonding to the ligands, therefore signifying a possibility for compounds up to a bond order of five, for species with a total of ten metal based electrons.[2]

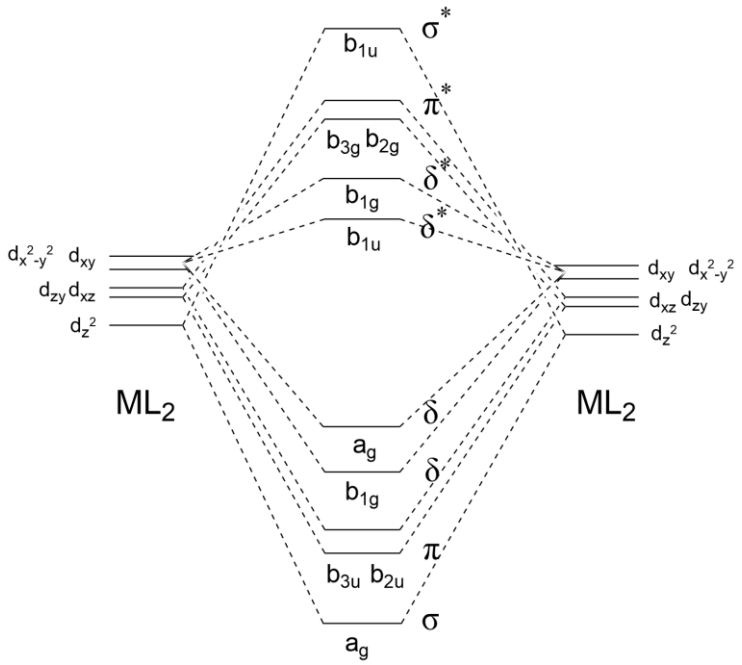

Figure 1.3. Model of the electronic configuration for a M_2L_2 complex in a D_{2h} conformation.

In order to be able to stabilize metal-metal bonds in different configurations, it is important to take a closer look at the ligands and their properties. Bulky monoanionic bidentate ligands (carboxylates, formamidinates, amidinates, guanidinates) are the most commonly used ligands in stabilizing bimetallic centers with high oxidation states. It has been proved that another important asset of a ligand to serve as a stabilizing agent is to possess a high basicity, therefore making guanidinates and formamidinates a focus of intense study. Scheme 1.1 shows the ligands used in this study.[3-5]

For the sake of understanding and gaining insight in the chemical properties of compounds with a D_{4h} and a D_{2h} symmetry, complete studies consisting of crystallographic studies, Electron Paramagnetic Resonance, Nuclear Magnetic Resonance, Raman and Infra-red spectroscopy, magnetism, electrochemistry and computational studies are presented .

In the first study, the structural and magnetic properties of four ruthenium bimetallic complexes, with the general formula $Ru_2(DarF)_4X$ (DarF = diarylformamidinate with Ar = *p*-anisyl or *m*-anisyl and X = Cl^- or BF_4^-), were compared under variable-temperature conditions.

The variations between these complexes included the change of ligand (i.e. making it more basic by changing the substituents from the *meta* to the *para* position) and the removal of an axial ligand. Data obtained gave insight on how the second variation can modify the electronic structure by proving the importance of a π interaction between the metal and the ligand.

On the second study presented, a tungsten bimetallic compound with the formula $W_2(TPG)_2Cl_4$ (TPG = triphenylguanidinate), was successfully synthesized and characterized. A bond order of three was confirmed by cyclic voltammetry and single crystal X-ray crystallography. The first reduction of the compound, with a bond order of 3.5, was achieved and was further studied by EPR and Raman spectroscopy.

Scheme 1.1 Drawings of HDanimF, HDanipF and HTPG, ligands used in this study

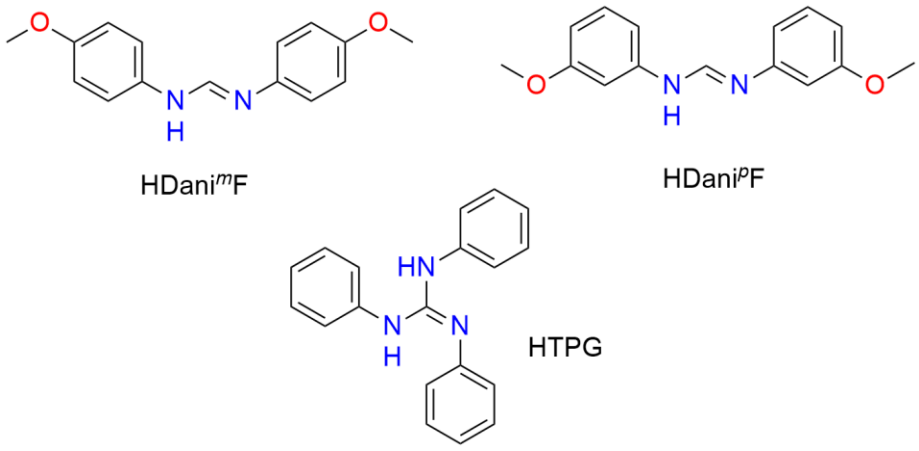

Chapter 2: Manipulating Magnetism: Ru_2^{5+} Paddlewheels devoid of axial interactions.[†]

1. Introduction

While the occurrence of π interactions between ligand and metal atoms has long been known to occur,[6] it is not often that unambiguous evidence can be found, especially in complexes containing transition metal species. Here we describe much evidence to support their effect, albeit found in a nontraditional place, that is, diruthenium paddlewheel compounds with metal–metal bonds.

Reports from different laboratories[7] have drawn attention to the way structural data over a wide temperature range can provide valuable information and heretofore unutilized evidence pertaining to the electronic structures of paddlewheel compounds having Ru_2^{5+} cores in particular. One of the enticing but frustrating features of such compounds, of which the earliest were of the type $Ru_2(O_2CR)_4Cl$,[8] is that their frontier molecular orbitals are usually very similar in energy.[9,10] Even small variations in their relative energies can lead to significant changes in their electronic structure, which affects the corresponding metal–metal distances[10,11] and magnetism.[12] Because of the similarity in energy between the highest occupied molecular orbital (HOMO) and the singly occupied molecular orbital (SOMO), the provenance of the ground state for these species with an 11-electron core might be any of three configurations, $Q\delta^{*2}\pi^*$, $Q\pi^{*2}\delta^*$, $Q\pi^{*3}$ (where Q represents the underlying $\sigma^2\pi^4\delta^2$ quadruple bond configuration).[13] Moreover, two states that each arise from a different one of these configurations (which have bond orders of 2.5) might be so close in energy that a Boltzmann-type temperature dependence of their partial

[†] This chapter previously appeared as an article in the Journal of the American Chemical Society. The original citation is as follows: Chiarella, G. M.; Cotton, F. A.; Murillo C. A.; Ventura, K.; Villagrán, D.; Wang, X, Manipulating Magnetism: Ru_2^{5+} Paddlewheels devoid of axial interactions. *J. Am. Chem. Soc* ,**2014**, *136* (27), pp.9580-9589

populations could come into play. For these configurations, magnetic measurements may distinguish between the $Q\pi^{*2}\delta^*$ state, which has three unpaired electrons, but not the other two ($Q\delta^{*2}\pi^*$and $Q\pi^{*3}$) which have one unpaired electron each.The temperature dependence, or absence thereof, of the Ru–Ru bond length can show whether or not close-lying states that derive from different configurations are involved, and if so, which pairs of configurations are pertinent. For example,[7b] the combination of the magnetic and structural data for $Ru_2(DAni^pF)_4Cl$, **1**, ($DAni^pF$ = *N,N'*-di-*p*-anisylformamidinate shown in Scheme 2.1) lead to the certain conclusion that there is a ground state (^2E_g) derived from the $Q\pi^{*3}$ configuration (11 metal-centered

Scheme 2.1. $HDAni^pF$, $HDAni^mF$, HDPhIP, HPhIP, Ligands Cited in the Text.

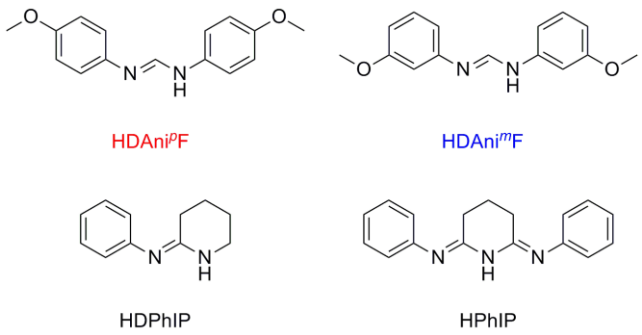

electrons) and a low-lying excited state ($^4B_{2u}$) derived from the $Q\pi^*2\delta^*$ configuration (Scheme 2.2). In the same report it was shown that the meta isomer $Ru_2(DAni^mF)_4Cl$, **2**, where the ligand is less basic than that of the para isomer, the $Q\pi^{*2}\delta^*$ configuration persists at all temperatures between 27 and 300 K. Although there is a strong temperature-dependence of the magnetism due to zero-field splitting (ZFS), in which the magnetism seemingly drops from an equivalent of three unpaired electrons to an apparent state with only one unpaired electron, the Ru–Ru distance is essentially temperature-independent. An axial chlorine atom is present in both of these isomers, and it was only the basicity of the DArF ligands (where DArF is the anion of a diarylformamidine isomer, and Ar = *p*-anisyl or *m*-anisyl) in **1** and **2** that changed. It should also be mentioned that in another crystal having two crystallographically distinct but chemically

similar molecules with Ru_2^{5+} cores and slightly different intermolecular interactions to axial ligands, the two molecules behaved very differently as the temperature was lowered. The Ru–Ru distances changed for one of the molecules but not for the other molecule.[14]

Scheme 2.2 Electronic Splitting Diagram for an 11 electrons Bimetallic Unit Metal- with An Idealized D4h Symmetry**.**

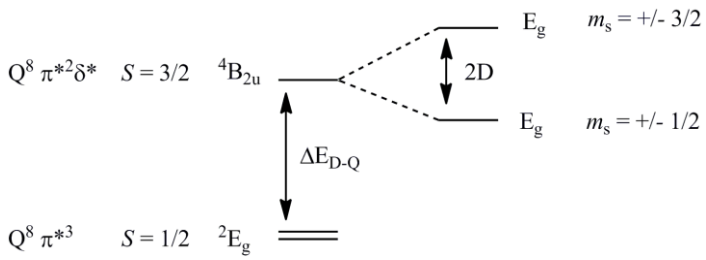

Here, the consequences of two other variations in compounds of the $Ru_2(DArF)_4X$ type are explored (DArF = *N*,*N'*-diarylformamidinate): (1) what happens when the same DArF bridges are retained, but the axial chloride species are replaced by the essentially noncoordinating BF_4^- anion;[15] and (2) what happens when the aryl group (Ar) in DArF is changed from *p*-Ani to *m*-Ani (Ani = anisyl) in $[Ru_2(DArF)_4]BF_4$ to form two species devoid of axial coordination, namely, $[Ru_2(DAni^pF)_4]BF_4$, **3**,and $[Ru_2(DAni^mF)_4]BF_4$, **4**.The existence of pairs of compounds with identical cores for which one of the members of the pair has an axial ligand while the other one is naked, allows for the first time an unambiguous analysis of the effect of axial ligation in Ru_2^{5+} species. As discussed below the results are consistent with significant π interactions of the axial Cl groups with the diruthenium units in the $Ru_2(DArF)_4Cl$ species.

2. Experimental

Unless otherwise noted, all syntheses were carried out under inert atmosphere using standard Schlenk techniques. The ligand precursors $HDAni^pF$ and $HDAni^mF$ were prepared by the general thermolysis reaction of triethylorthoformate in the presence of the corresponding aniline at 130

°C over 4 h, followed by extensive washing of the solids with pentane before their use.[40] The diruthenium $Ru_2(OAc)_4Cl$ precursor was prepared as previously reported.[41] Compound **1** was prepared according to an established synthetic procedure.[42] Solvents were dried using a Glass Contour solvent system. Elemental analyses were performed by Robertson Microlit Laboratories, Inc., Madison, NJ. Infrared spectra were recorded in a Perkin Elmer 16PC FT-IR spectrophotometer using KBr pellets. The X-band (~9.5 GHz) variable-temperature EPR spectra were obtained using a BrukerEMX plus spectrometer with an ER073 magnet equipped with a cryogen-free 10° FlexLine system. All samples were measured in frozen toluene (glasses) at 10 K. To increase solubility of **2** and **4** in toluene, a couple of drops of dichloromethane were added to the EPR samples. Variable-temperature magnetic susceptibility measurements were obtained from 2 to 300 K using a Quantum Design SQUID magnetometer MPMS-XL operated at 1000 G. These data were corrected for diamagnetism using Pascal's constants.[43]

2.1. Synthesis of $[Ru_2(DAni^mF)_4]Cl$, 2.

In a 100 mL round-bottomed flask equipped with a condenser and a magnetic stirring bar, $Ru_2(OAc)_4Cl$ (0.961 g, 2.00 mmol), $HDAni^mF$ (4.10 g, 16.0 mmol), triethylamine (5 mL), and an excess of anhydrous LiCl (2.0 g) were mixed in 50 mL of THF which had been degassed via freeze-thawing. The mixture was heated to reflux under nitrogen for 48 h. The solvent from the dark green mixture was then removed under vacuum. The solid was washed with water to remove LiCl and then extracted with CH_2Cl_2 and further purified using a silica gel column and a mixture of hexanes, CH_2Cl_2 and acetone as eluent. From this point on, the compound was no longer protected from air. A fraction contained in a dark band was collected and the solvent was then removed under vacuum to produce 2.36 g of a green solid. Yield: 85%. Crystals suitable for X-ray analysis were obtained by slow diffusion of hexanes into a CH_2Cl_2 solution of the product.

Anal. Calcd for $C_{60}H_{60}N_8O_8ClRu_2$: C, 57.25; H, 4.80; N. 8.90%. Found: C, 57.61; H, 4.80; N, 8.71%. IR (KBr pellet, cm^{-1}): 1600, 1534, 1482, 1466, 1327, 1283, 1265, 1195, 1152, 1081, 1038, 983, 939, 858, 774, 757, 695, 522 and 449.

2.2. Synthesis of $[Ru_2(DAni^pF)_4]BF_4$, 3.

To a solution of $Ru_2(DAni^pF)_4Cl$ (0.255 g, 0.200 mmol) in 20 mL of CH_2Cl_2 was added a stoichiometric amount of $TlBF_4$. The mixture was stirred overnight at room temperature. The mixture was then filtered through Celite to remove the insoluble TlCl. The volume of the bluish solution was reduced to about 5 mL, and then layered with hexanes to yield single crystals of X-ray diffraction quality. Anal. Calcd for $C_{60}H_{60}N_8O_8BF_4Ru_2$: C, 55.01; H, 4.62; N. 8.55%. Found: C, 54.77; H, 4.43; N. 8.61%. IR (ATR, cm^{-1}): 1605, 1496, 1459, 1392, 1253, 1186, 1081 (BF_4^-), 1030, 724, 693.

2.3. Synthesis of $[Ru_2(DAni^mF)_4]BF_4$, 4.

A salt metathesis reaction similar to that used for the synthesis of **3** was utilized. Yield: 93%. Anal. Calcd for $C_{60}H_{60}N_8O_8BF_4Ru_2$: C, 55.01; H, 4.62; N. 8.55%. Found: C, 54.66; H, 4.61; N, 8.29%. IR (KBr pellet, cm^{-1}): 1582, 1522, 1482, 1444, 1305, 1287, 1265, 1197, 1156, 1083, 1056 (BF_4^-), 1039, 985, 943, 845, 762 and 691.

2.4. Computational Details.

DFT[44] calculations were performed with the hybrid Becke-3[45] parameter exchange functional and the Lee−Yang−Parr[46] nonlocal correlation functional (B3LYP) as implemented in the Gaussian 03 program suite.[47] Double-ζ-quality basis sets (D95)[48] were used on nonmetal atoms (carbon, nitrogen and hydrogen) except for Cl (6-311g(d)). An effective core potential (ECP)[49] representing the 1s2s2p3s3p3d core was used for the ruthenium atoms along with the associated double-ζ basis set (LANL2DZ). A second set of calculations using the modified

version of LANL2DZ by Couty and Hall to the ruthenium atoms was applied for redundancy and comparison.[50] The convergence criterion for the self-consistent field cycles on all calculations was increased from the default value to 10^{-8}. Geometry optimization calculations were found to be minima in the potential energy surface as evidenced by the lack of imaginary vibrations in the frequency calculations.

2.5. X-ray Structure Determinations.

Crystals of **3** and **4** were coated with Paratone oil and mounted on a nylon Cryoloop affixed to a goniometer head. Data for **3** and **4** were collected on a Bruker SMART 1000 charge-coupled device (CCD) area detector system using omega scans of 0.3 deg per frame, with exposures of 30, 10 and 10 s per frame at 27, 200 and 298 K, respectively. The exposure rates for **4** were 20 s per frame at the temperatures of 33, 100, 213, and 298 K. Cell parameters were determined using the SMART software suite.[51] Data reduction and integration were performed with the software SAINT.[52] Absorption corrections were applied using the program SADABS.[53] The positions of the Ru atoms were found via direct methods using the program SHELXTL.[54] Subsequent cycles of least-squares refinement followed by difference Fourier syntheses revealed the positions of the remaining non-hydrogen atoms. Hydrogen atoms were added in idealized positions. All hydrogen atoms were included in the calculation of the structure factors. All non-hydrogen atoms were refined with anisotropic displacement parameters. In **3**, half of the atoms in the DAni^{p}F ligands were disordered. The disorder in the four ligands was successfully treated with a major component varying from 74.9 –79.8% and a minor component of 20.2 – 25.1% depending on the temperature at which the data were collected. The tetrafluoroborate anion was also disordered and the structure was refined in the orthorhombic space group $Pna2_1$. For **4**, the structure refinement was done in the tetragonal space group $P4/nnc$ instead of the lower-symmetry space

group *P*4/*n* that suggested by the XPREP program. This was done following Marsh's recommendations.[55] Data collection and refinement parameters for **3** and **4** are summarized in Table 2.7. Selected bond distances and angles are listed in Tables 2.1 and 2.3.

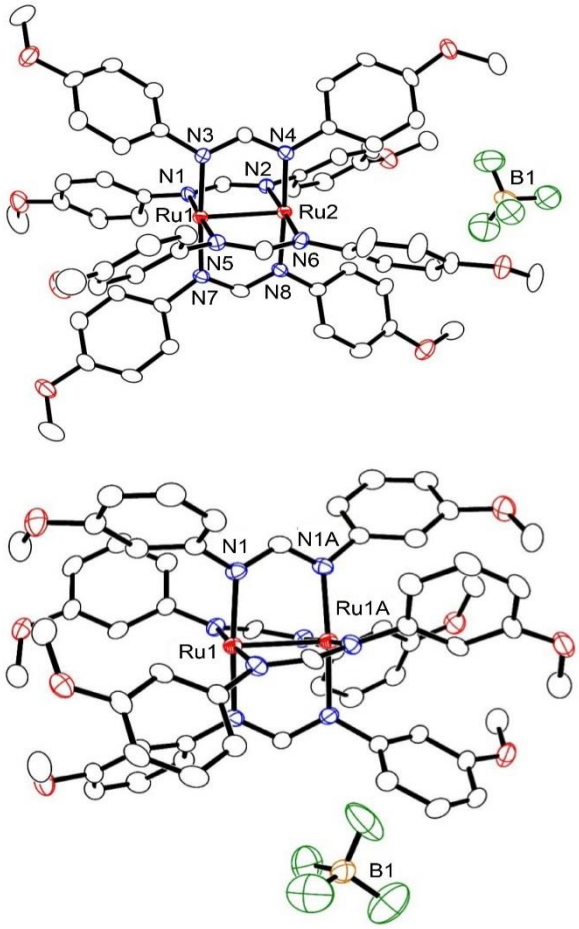

Figure 2.1 Crystal structures at 213 K of the isomers $[Ru_2(DAni^pF)_4]BF_4$ (**3**, top) and $[Ru_2(DAni^mF)_4]BF_4$ (**4**, bottom) drawn with displacement ellipsoids at the 30% probability level. Hydrogen and disordered atoms have been omitted for clarity.

3. Results and Discussion

3.1. Syntheses.

The preparation of the $Ru_2(DArF)_4Cl$ compounds **1** and **2** was accomplished in tetrahydrofuran (THF) by reaction of $Ru_2(OAc)_4Cl$ with the corresponding diarylformamidine in the presence of triethylamine to aid the deprotonation process and anhydrous LiCl to promote the ligand substitution reaction. Substitution of the axial chlorine atoms from the $Ru_2(DArF)_4Cl$ compounds, to produce **3** and **4,** was carried out by addition of a solution of $TlBF_4$ in the noncoordinating solvent CH_2Cl_2,[11] followed by removal of insoluble thallium chloride:

$Ru_2(O_2CCH_3)4Cl + 4HDArF + LiCl \rightarrow Ru_2(DArF)_4Cl + 4HO_2CCH_3$

$Ru_2(DArF)_4Cl + TlBF_4 \rightarrow [Ru_2(DArF)_4]BF_4 + TlCl$

3.2. Structure and Magnetism.

As noted, the substitution of the axial groups in $Ru_2(DArF)_4Cl$ type compounds by noncoordinating anions in the absence of other possible coordinating species allows exploration of the consequences of two other variations in compounds of the $Ru_2(DArF)_4X$ type: (1) the effect of retaining the same DArF bridges being retained while the axial chloride species are replaced by the essentially noncoordinating BF^{4-} anion; and (2) the effect of small basicity effects of the Ar being changed from *p*-Ani to *m*-Ani in $[Ru_2(DArF)_4]BF_4$ isomers.[17]

Variation (1). Structures of $[Ru_2(DAni^pF)_4]BF_4$, **3**, one of which is shown in the upper section of Figure 2.1, were determined at 27, 200 and 298 K, and principal bond lengths at each of those temperatures are provided in Table 2.1. The Ru–Ru distance is in the range 2.4000(5)–2.4078(7) Å at all measured temperatures, and this is consistent with the structure of the Ru_2N_8 core in **3** being temperature-independent. These results contrast with those for **1**,[7b] where the Ru–Ru

distance decreased by about 0.05 Å, from 2.4471(5) Å at 27 K to 2.3968(5) Å at 300 K (Table 2.2). The cation in **3**, which is devoid of axial interactions,[18] represents the first structurally characterized example of a naked Ru_2^{5+} paddlewheel compound.[19]

Structures for $[Ru_2(DAni^mF)_4]BF_4$, **4**, one of which is shown at the bottom of Figure 2.1, were determined at 33, 100, 200 and 298 K. Again, the Ru–Ru distance in the cation remains constant and in the range of 2.389(4) to 2.3839(4) Å. Selected results of the variable-temperature (VT) crystallographic studies are shown in Table 2.3 and Figure 2.2. Similarly to **3**, it is again clear that the structure of this axially naked species is temperature independent, and thus its electronic structure is invariant with respect to temperature. In this aspect, **4** resembles the axially chlorine-ligated **2**;

However, the corresponding Ru–Ru distance varies by ~ 0.05 Å, with that of **2** being shorter than that of **4**.

Table 2.1 Selected Bond Distances and Angles for **3** at Three Temperatures.

	3[a]	**3**[b]	**3**[c]
Ru1–Ru2	2.4078(7)	2.4069(7)	2.4000(5)
Ru1–N8	2.038	2.038	2.029
Ru1–Ru2–N4	88.9	88.8	88.8
Ru2–Ru1–N4	88.7	88.7	88.9

[a]27 K. [b]200 K. [c]298 K.

The magnetism of **3** is consistent with an S = ½ state over the range of 2 K to ambient temperature, as shown in Figure 2.3. This is also in sharp contrast to that of **1,** which shows three unpaired electrons at room temperature with a χT value that reaches a maximum of 1.6 emu·K·mol^{-1} at 300 K and declines to a minimum of 0.5 emu·K·mol^{-1} at 2 K (red circles in Figure 2.3). This behavior has been

Table 2.2 Ru-Ru Bond Distances for **1** and **2** at Different Temperatures.

Temperature (K)	**1**	**2**[b]
27	2.4471(5)	2.3333(3)
60	2.4397(6)	-
100	2.4289(5)	2.3326(3)
150	2.4168(5)	-
220	2.4019(5)	2.3376(3)[c]
299	2.3968(5)	2.3398(4)

[a]See ref. 7a

[b]Data at 60 and 150 K not collected.

[c]Collected at 213 K.

attributed to a spin-crossover process from a doublet ground-state derived from a $Q\pi^{*3}$ at low temperatures to a spin quartet state derived from a $Q\pi^{*2}\delta^{*}$ configuration.[7b] The magnetism of **3** also differs from also that of **2**, which follows a commonly observed decrease in the χT attributable to ZFS for a $^4B_{2u}$ state derived from a $Q\pi^{*2}\delta$ configuration (Scheme 2.2) that is frequent in Ru_2^{5+} species.[12a,20,21] For **4**, the magnetism resembles that of **3** also having one unpaired electron and χT value being constant (0.35 ± 0.02 emu·K·mol^{-1}) from 2 to 300 K. This data can be modeled by the Curie law ($\chi = ((Ng^2\beta^2)/(3kT))S(S + 1)$) with the fitted values of g of 1.925(4) and 2.000(5) for **1** and **2**, respectively, where N is Avogadro's number, β is the Bohr magneton, k is the Boltzmann constant and T is the temperature in Kelvin.

To explain the difference in structural and magnetic properties of **1** and **3**, the interactions of the axial chloride ion in **1** with the Ru_2^{5+} core must be considered. The structural and magnetic data suggest that **1**, at low temperature, and **3** at all measured temperatures are in the ^2E_g state arising from the $Q\pi^{*3}$ configuration (Scheme 2.2). The reason that **1** has a longer Ru–Ru distance in this state is because, as is commonly found in paddlewheel compounds with metal–metal bonds,[10] an axial σ donor weakens the metal–metal σ bonding. The fact that **3** remains in the ^2E_g state as the temperature rises to 300 K indicates the separation between the ^2E_g state and the lowest state arising from the $Q\pi^{*2}\delta^{*}$ configuration (Scheme 2.2) is above the value

of kT at 300 K (i. e.,≥ 600 cm^{-1}). Contrarily, this separation must be smaller in **1** than in **3**. The reason for this difference in magnetism must be attributed to a destabilization of the energy of the π^* orbitals by the axial Cl^- ligand attached to the $[Ru_2(DAni^pF)_4]^+$ core while (because of symmetry incompatibility) there is no direct effect on the δ^* orbital.

Table 2.3 Selected Bond Distances and Angles for **4** at Different Temperatures

	4[a]	**4**[b]	**4**[c]	**4**[d]
Ru1–Ru1A	2.389(4)	2.383(4)	2.3879(19)	2.3859(14)
Ru1–N1	2.065(7)	2.041(7)	2.035(5)	2.033(4)
Ru1–Ru1A–N1	88.2(2)	87.8(2)	88.18(15)	88.30(11)

[a]33 K. [b]100 K. [c]213 K. [d]298 K.

The difference in Ru–Ru bond distances between **2** and **4** can be explained by invoking a similar argument. These compounds have different electronic configurations, $Q\pi^{*2}\delta^*$ and $Q\pi^{*3}$ for **2** and **4**, respectively. Because a π^* orbital has a greater antibonding character than a δ^* orbital, the $Q\pi^{*3}$ configuration is expected to be more repulsive than that in the $Q\pi^{*2}\delta^*$, and thus the Ru–Ru distance in **4** is longer than that in **2**.

Variation (2). When there is no significant axial ligation as in both of the $[Ru_2(DArF)_4]BF_4$ species **3** and **4**, the change from more basic $DAni^pF$ to the less basic $DAni^mF$,[17] has no major

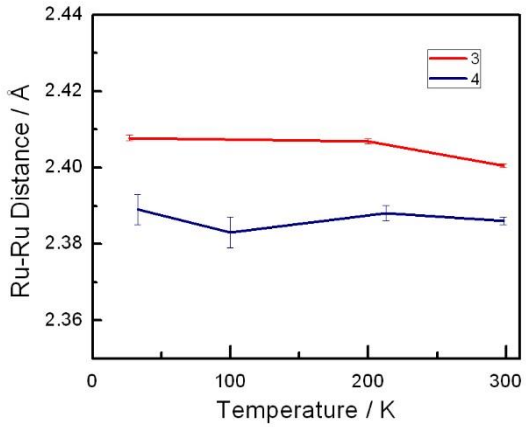

Figure 2.2 Change in Ru−Ru distances for **3** and **4**. The distances remain basically constant within the margin of error in the measured range of temperatures.

effect on the structure and magnetism. Nonetheless, there is a slight decrease of 0.019 Å in the Ru–Ru distance from 2.4069(7) in **3** at 200 K to 2.3879(19) Å in **4** at 213 K, but this distance is temperature-independent in both compounds. This result coupled with the fact that in each case χT is also temperature-independent and corresponds to one unpaired electron suggests that in each case a $Q\pi^{*2}\delta^{*}$ ground state as well as any temperature-dependent distribution over two states can be ruled out. The only remaining possibilities are that (1) a ^2E_g state arising from a π^{*3} configuration in either cases, or that (2) a $^2B_{2u}$ state arising from a $\delta^{*2}\pi^{*}$ configuration in the two cases.

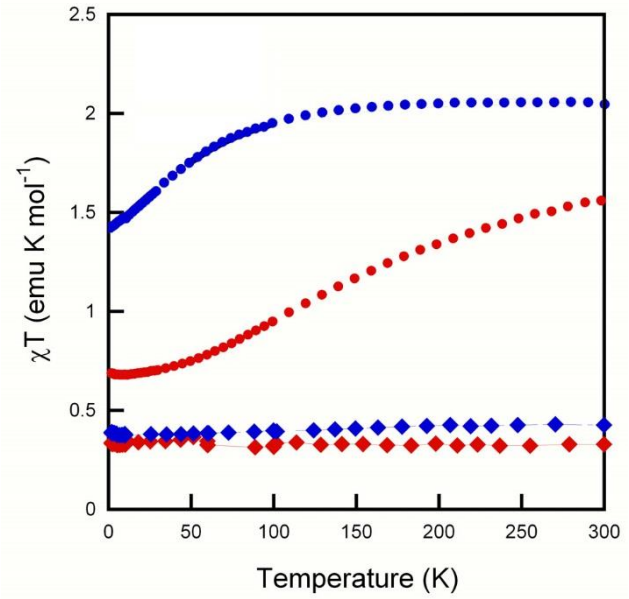

Figure 2.3 Magnetic susceptibility versus temperature of $Ru_2(DAni^pF)_4Cl$ (**1**, red circles), $Ru_2(DAni^mF)_4Cl$ (**2**, blue circles),$[Ru_2(DAni^pF)_4]BF_4$ (**3**, red diamonds), and $[Ru_2(DAni^mF)_4]BF_4$ (**4**, blue diamonds).

To decide between these two possibilities, the structure of the BF_4 compounds must be compared to those of the corresponding Cl compounds. In making these comparisons, we shall invoke two principal modes of interaction of the axial Cl^- ion with the Ru_2^{5+} core: (1) a σ donor

interaction that should weaken and hence lengthens the Ru–Ru bond and (2) a π donor interaction that will lower the energy of the π^* orbitals.

In the comparison of **3** and **1**, the shortening of the Ru–Ru distance[22] at 27 K by about 0.044 Å can be accounted on the basis of the first effect. On the basis of the second, the π^{*3} configuration would have increased stability compared to the $\pi^{*2}\delta^*$ and thus the latter would remain unpopulated even at 300 K in **3**.

In the comparison **4** and **2**, the rather large increase (0.052 Å, Table 2.4) in the Ru–Ru distance upon removal of the axial Cl^- is the opposite of what simple loss of a σ donor interaction would produce; however, an increase would result from a change from a $\pi^{*2}\delta^*$ configuration in **2** to a π^{*3} configuration in **4**. If the change in configuration from **2** to **4** were from $\pi^{*2}\delta^*$ to $\delta^{*2}\pi^*$ there would be no apparent explanation for the bond length increase since a δ^* orbital is expected to be less destabilizing than a π^* orbital. Indeed, in one of the very few characterized

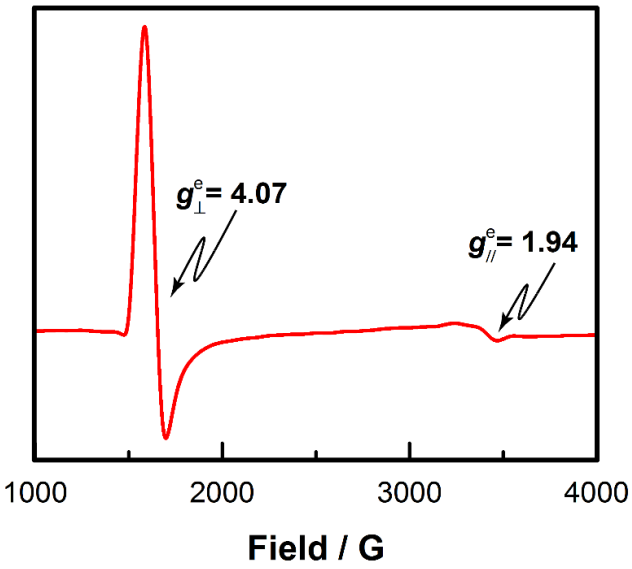

Figure 2.4 X-band EPR spectrum measured on a frozen toluene solution of **1** at 10 K, demonstrating that the unpaired spins are in an anisotropic environment and that the unpaired electrons are in metal-based MOs.

compounds with an Ru_2^{5+} core having a $Q\delta^{*2}\pi^*$ electronic configuration, $Na_3[Ru_2(Cl_4Cat)_4(THF)]$, where Cl_4Cat = tetrachlorocatecholate, which has two non-bridging catecholate ligands and an axial THF molecule, the unsupported Ru–Ru distance shown in Table 2.4 is only 2.273(1) Å,[23] and this distance decreases even further upon a one-electron oxidation that leads to removal of the electron in the π^* orbital to 2.2233(6) Å.[23]

Table 2.4. Electronic Configurations for Some Related Ru_2^{5+} Complexes**.**

	1 Cl/para	**3** BF_4/para	**2** Cl/meta	**4** BF_4/meta	**5** Cl/D(3,5-Cl_2Ph)F[a]	**6** Cl/Pr^nCO_2	$[Ru_2(DPhF)_3(OAc)(CH_3CN)]BF_4$[b]	$Ru_2(DPhF)_3(OAc)Cl$
Ru–Ru(Å)	2.4471(5) (27 K) 2.3968(5) (298 K)	2.4078(7) (27 K) 2.4000(5) (298 K)	2.333(3) (27 K) 2.3398(4) (298 K)	2.389(4) (33K) 2.3859(4) (298 K)	2.360(1) (27 K) 2.368(1) (300 K)	2.281(4)	2.4131(5)	2.3248(13)
Electronic configuration	π^{*3} ($\rightarrow\pi^{*2}\delta^*$)	π^{*3}	$\pi^{*2}\delta^*$	π^{*3}	$\pi^{*2}\delta^*$	$\pi^{*2}\delta^*$	π^{*3}	$\pi^{*2}\delta^*$
Ru–Cl(Å)					2.38	2.59		
Ru–Cl' or Ru–OH_2(Å)					2.63	2.59		
Ref.	7b	This work	7b	This work	12e	8b	32	31

[a] $[Ru_2(D(3,5\text{-}Cl_2Ph)F)_4Cl(0.5H_2O)]\cdot C_6H_{14}$, where D(3,5-$Cl_2$Ph)F = the anion of *N*,*N*'-di(3,5-dichlorophenyl)formamidine. [b] DPhF = the anion of *N*,*N*'-diphenylformamidine

3.3. Electron Paramagnetic Resonance Studies.

Electron paramagnetic resonance (EPR) spectra that were recorded in a toluene glass of **1–4** were obtained to further explore their electronic structures and the effects of their respective axial interactions. Compounds **1** and **2** are EPR silent at room temperature because of the large ZFS arising from the splitting of the $M_S = 0$ and $M_S = 3/2$ Zeeman levels. This is in agreement with the observed magnetic susceptibility measurement data. At low temperatures (10 K), highly anisotropic EPR signals were clearly discerned (Figures 2.4, and Figure 2.6). The signal for **1** in Figure 2.4, shows two *g*-tensor components because of the strong axial anisotropy, suggesting that the unpaired electrons reside in anisotropic environments and also supporting the occurrence of large ZFS. The spectrum for **2** (Figure 2.6) is similar to that for **1**. This suggests that **1** and **2** have similar electronic structures in solution. For **1** the effective g^e values of $g^e_\perp$ = 4.07 and $g^e_\parallel$ =

1.94 correspond to isotropic g values of 2.00, while for **2** the effective g values of $g^e_\perp$ = 4.09 and $g^e_\parallel$ = 1.94 corresponding to an isotropic g values of 2.01.[24] Consequently, the actual values for compound **1** are $g_\perp$ = 2.035 and $g_\parallel$ = 1.94, and the actual values for **2** are $g_\perp$ = 2.045 and $g_\parallel$ = 1.94.

When axial interactions in these isomers are removed as in **3** and **4**, the EPR signals drastically change. Figure 2.5 and Figure 2.7 show the low temperature EPR spectrum of **3**, and **4**, respectively. The spectra of **3** and **4** show only one signal at 2.01, and 1.99, respectively. According to the magnetic data (vide infra) **3** and **4** have a spin state of S = ½, therefore, no ZFS is expected and only isotropic signals are indeed observed.

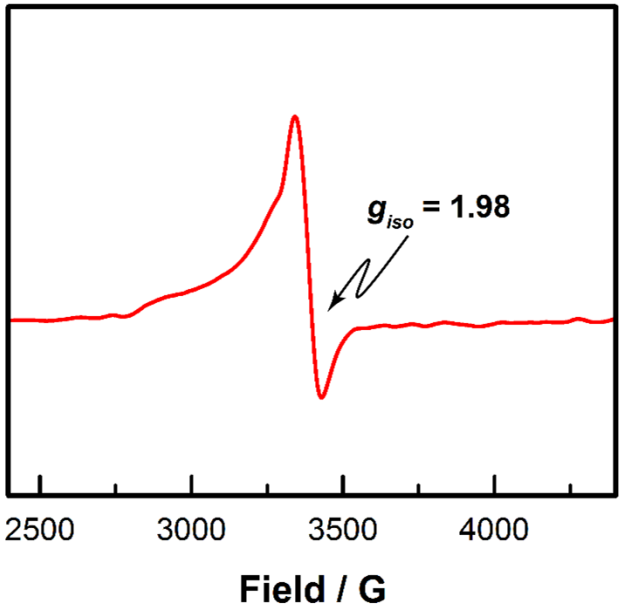

Figure 2.5 X-band EPR spectrum measured on a frozen toluene solution of **3** at 10 K

3.4.Comparisons to Other Dimetal Systems.

Two additional well-studied dimetal cores that are affected by axial ligands are those having M_2^{4+} species, M = Cr and Rh.[25] For Cr it was not until about a decade ago that the first

$Cr_2(O_2CR)_4$ compound without axial ligands was isolated.[26] The Cr–Cr distance of 1.9662(5) Å is significantly shorter than those in other $Cr_2(O_2CR)_4L_2$, L = donating ligand, which have Cr–Cr distances about 0.4 Å longer. For the rhodium analogues, $Rh_2(O_2CR)_4L_2$, which have Rh–Rh distances in the range of 2.34–2.41 Å,[25,27] the change in the metal–metal bond is not as large, for the compound without axial ligands this distance is 2.3499(4) Å.[28]

An additional pair of compounds that provide a relevant comparison is represented by $Cr_2(DPhIP)_4$ and $Cr_2(PhIP)_4$ (DPhIP = the anion of 2,6-di(phenylimino)piperidine and PhIP = the anion of 2-(phenylimino)piperidine, shown at the bottom of Scheme 2.1). Both of these

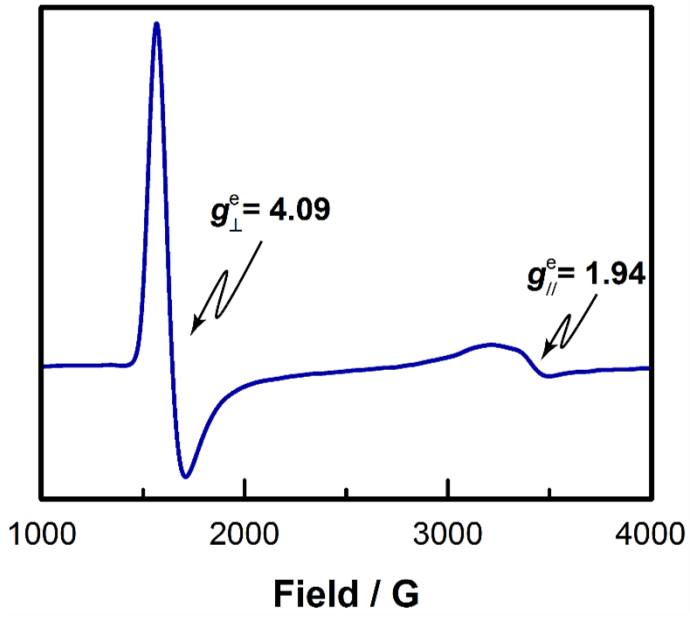

Figure 2.6 X-band EPR of **2** in toluene glass at 10 K.

paddlewheel compounds have a Cr_2N_8 core yet the Cr–Cr distances differ by ca. 0.41 Å, being 2.265(1) Å in $Cr_2(DPhIP)_4$ and 1.858(1) Å in $Cr_2(PhIP)_4$.[29] The difference has been attributed to the four imino nitrogen lone pairs in the DPhIP ligands that are positioned to donate to the π^* orbital of the Cr_2^{4+} unit at distances of about 2.73 Å, while $Cr_2(PhIP)_4$ is devoid of such interactions.

More recently, an analogous effect was reported involving the axial interactions of the triple bonded $[W_2(hpp)_4]^{2+}$dication (hpp = the anion of 1,3,4,6,7,8-hexahydro-*2H*-pyrimido[1,2-a]pyrimidine), which is the precursor of $W_2(hpp)_4$, a thermally stable molecule with a very low ionization energy. In halogenated solvents, $W_2(hpp)_4$ is easily oxidized to $W_2(hpp)_4Cl_2$.[31] This compound has very long W···Cl distances of about 3.0 Å but DFT calculations showed that even at those long axial distances, strong repulsive interactions exist between the metal–metal and the Cl ligand pσ_s occupied orbitals.[30] A related effect has also been observed in analogous compounds having Re_2^{6+} cores.[32]

Another pair of compounds pertinent to the present discussion involve $Ru_2(DPhF)_3(OAc)Cl$[33] and $[Ru_2(DPhF)_3(OAc)(acetonitrile)]BF_4$[34] (DPhF) = *N*,*N*′-diphenylformamidine). Both compounds have an Ru_2^{5+} core surrounded by four bridging ligands (a mix of formamidinate and acetate ligands) and a paddlewheel structure akin to **1**–**4**. The compound $Ru_2(DPhF)_3(OAc)Cl$ also has one axial halogen atom similar to those of **1** and **2**. The species $[Ru_2(DPhF)_3(OAc)(acetonitrile)]BF_4$, unlike **3** and **4** has an axial CH_3CN molecule. It should be

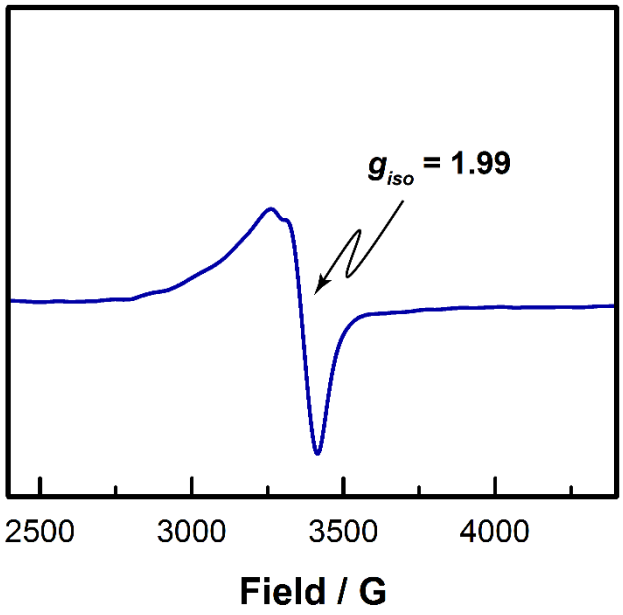

Figure 2.7 X-band EPR spectrum of **4** toluene glass at 10 K

noted that the acetonitrile molecule is a good σ donor but not a π donor and this explains why the Ru–Ru distance in the acetonitrile compound increases by ca. 0.09 Å (Table 2.4) relative to that of the chlorine-containing compound. This is consistent with the hypothesis provided in the Variation (2) section above. It should be noted that Jiménez-Aparicio et al. have also reported a series of additional $Ru_2(DPhF)_3(OAc)L_{ax}$, L_{ax} = $OPMe_3$, H_2O, 4-picolinate, and CO that clearly shows that the nature of the axial ligand, L_{ax}, affects the Ru–Ru bond distance.[35] Some of the distances for compounds in this family are shown in Table 2.5.

Table 2.5 Distances (Å) for a Family of Paddlewheel $[Ru_2(DPhF)_3(OAc)Lax]^+$ Species with Ru_2^{5+} Cores and Mixed Diphenylfomamidinate and Acetate Paddles.

L_{ax}	Ru–Ru
$OPMe_3$	2.303
Cl	2.3248
H_2O	2.350
4-picolinate	2.408
acetonitrile	2.4131
CO	2.450

[a] Note that as the π acceptor capability of the ligand (e. g., in CO) increases, the gap between π* and δ* orbitals increase favoring the $Q\pi^{*3}$ electronic configuration. This lowers the magnetism and also there is a concomitant increase in the metal-to-metal distance.

3.5. DFT Calculations.

To qualitatively investigate the effect of the axial interactions on the electronic structure of these $[Ru_2(DAniF)_4]^+$ systems, a series of DFT calculations based on models of the axially ligated **1** and **2** and the axially naked **3** and **4** were used, and the relative energies of the optimized geometries of the doublet and quartet multiplicities of each model were calculated. In the models, the aryl groups in the bridging formamidinate ligands were replaced by H atoms. These simplifications were done to reduce the computation expense; however, it is important to note that such simplifications do not significantly compromise the modeling of the electronic

structure, as shown before.[36] Two different multiplicities (doublet and quartet) were calculated for the models of the axially chlorine-ligated species **1** and **2**, and for the models of the axially-naked $[Ru_2(DAniF)_4]^+$ species **3** and **4**. The calculated total energies of the geometry optimized models are given in Table 2.6. A comparison of the relative energies of the doublet (S = ½) and quartet (S = 3/2) states that the axially chlorine-ligated model indicates that the quartet state is more stable than the doublet state by about 1.4 kcal/mol. This small energy difference is consistent with the experimentally observed behavior of **1**, which shows temperature dependent spin-crossover.[2b] By contrast, the energy difference between the doublet and the quartet states in the axially devoid model shows that the doublet state is favored over the quartet state by about 5.4 kcal/mol as shown in Table 2.6.[37] This is a significantly larger energy difference than that was calculated for the axially chlorine-ligated model and is consistent with the observed magnetism of **3** and **4**, which shows a doublet state at all temperatures. This energy difference between the doublet and quartet states from the two different systems (axially ligated, and naked)

Table 2.6. Energies from DFT for the Calculated Models

Model	Multiplicity	*S*	Energy (hartrees)	ΔE_{d-q}(kcal/mol)
Axially ligated Cl	Doublet	½	–1245.7696034	–1.40
	Quartet	3/2	–1245.7718294	
Axially naked	Doublet	½	–785.297632398	5.44
	Quartet	3/2	–785.288961454	
Axially ligated with long Cl[a]	Doublet	½	–1245.68693350	6.21
	Quartet	3/2	–1245.67703316	

[a] Not geometry optimized but using the axially-naked geometry

suggests that the doublet state is stabilized by removal of the axial Cl^- anion. As mentioned earlier, this axial ligand interaction on Ru_2^{5+} systems had been previously noted.[35] Our calculations of the naked paddlewheel Ru_2^{5+} system support previous results, but the current calculations go beyond what have been done so far. The current set of calculations was carried out by manipulating the distances from a Ru atom to the axial Cl^- anion (either by shortening or lengthening them). In this way, it is possible to track the metal orbital energies as a function of

the axial $Ru_2\cdots L_{ax}$ separation. A qualitative diagrammatic representation of the metal–metal bonding manifold corresponding to the long and short axial Cl ligand distances is given in Scheme 2.3. On the left of the diagram the frontier orbitals (δ^* and π^*) show a quasi-degeneracy, but this quasi-degeneracy is broken as the axial Cl atom is removed (right). This effect is due to antibonding interactions between the Cl p orbitals and the orbitals of π symmetry of the diruthenium core. As the Cl anion leaves the axial site, the π^* metal–metal orbital is stabilized.[38] A quantitative estimate of the extent of this π^*orbital stabilization can be obtained by comparing the relative energies of the frontier orbitals of the axially Cl^- ligated model and a second

Scheme 2.3 Molecular Orbital Diagram. As the Ru···Cl separation increases the energy of the metal-based π orbitals quickly drop, increasing the π–δ gap

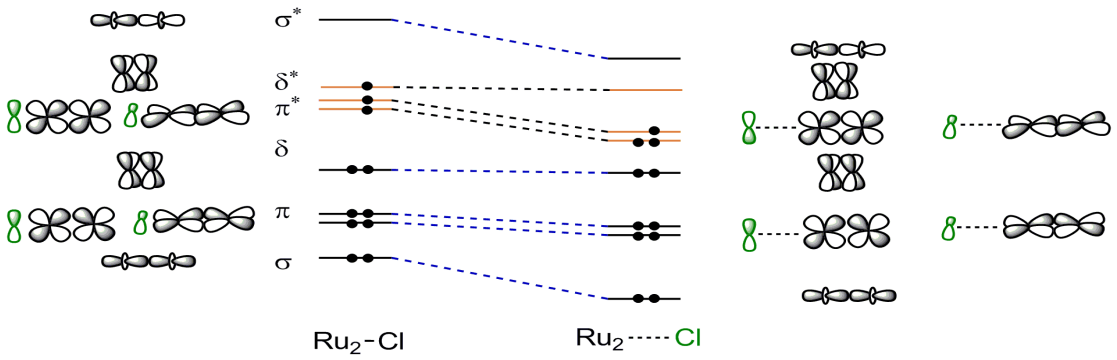

calculation that uses the optimized geometry of the axially naked Ru_2 model. In this model, the Cl^- anion was positioned at a distance of 8.0 Å from the diruthenium unit where no chemically meaningful $Ru_2\cdots Cl$ interaction would be expected. For this model, and consistent with the results from the axially-naked one, the doublet state is more stable than the quartet state by 6.21 kcal/mol (Table 2.6). Figure 2.8 shows a molecular orbital diagram constructed from the calculations of the ground state models at two different $Ru_2\cdots Cl$ separations. The quartet state model (depicted by the molecular orbitals (MOs) at the center of Figure 2.8) shows that the

metal-based π^* orbitals are about 1eV more stable than the δ^* orbitals. As the chlorine atom is pulled away (Figure 2.8, outer MOs) the energy separation between the π^* and δ^* orbitals increases to about 4.0 eV. Because of the long $Ru_2\cdots Cl$ distances in the doublet state case, the

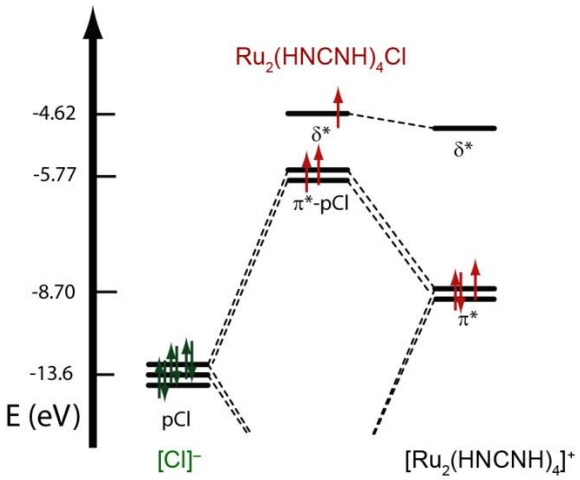

Figure 2.8 Molecular orbital diagram showing the construction of the frontier orbitals of the Cl^- axially ligated from the axially naked Ru_2^{5+} core and Cl^- ligand p orbitals. Note that the energy gap between the metal based π* and δ* significantly increases from R

p_{Cl} orbitals are isolated, and thus have energies similar to those expected for an outer sphere Cl^- anion. Figure 2.8 also shows that the metal-based π^* orbitals of the model with the long $Ru_2\cdots Cl$ separations are more stable in energy (by about 2.9 eV) than those with the shorter separations. Even though, the δ^* orbital is also stabilized by the $Ru_2\cdots Cl$ elongation, the drop in energy is relatively small compared to that of the π^* orbitals and thus the energy separation between the π^* and δ^* orbitals increases to 4.0 eV. Therefore, the calculations for the model with long $Ru_2\cdots Cl$ distances favor the doublet state by about 6.21 kcal/mol. In contrast, calculations for the model with short $Ru_2\cdots Cl$ distances favor the quartet state, mainly because of the smaller π^*–δ^* energy separation of ~1 eV.[39] This is consistent with the observed magnetism of **1** and **2**, which have short Ru_2–Cl distances and accessible quartet states, and contrasts with the observed

magnetism of **3** and **4**, which show only an accessible doublet state at all temperature and no Ru–L_{ax} interactions.

Table 2.7. Crystallographic Data for **3** and **4**

	3	**3**	**3**	**4**	**4**	**4**	**4**
chemical formula	$Ru_2C_{60}H_{60}N_8O_8BF_4$	$Ru_2C_{60}H_{60}N_8O_8BF_4$	$Ru_2C_{60}H_{60}N_8O_8BF_4$	$Ru_2C_{60}H_{60}N_8O_8BF_4$	$Ru_2C_{60}H_{60}N_8O_8BF_4$	$Ru_2C_{60}H_{60}N_8O_8BF_4$	$Ru_2C_{60}H_{60}N_8O_8BF_4$
formula weight	1310.11	1310.11	1310.11	1310.11	1310.11	1310.11	1310.11
space group	*Pna*2$_1$(No. 33)	*Pna*2$_1$ (No. 33)	*Pna*2$_1$ (No. 33)	*P*4/*nnc* (No. 126)	*P*4/*nnc* (No. 126)	*P*4/*nnc* (No. 126)	*P*4/*nnc* (No. 126)
a (Å)	34.572(6)	34.973(8)	34.973(8)	13.7952(18)	13.6662(11)	13.7952(18)	13.8927(5)
b (Å)	12.945(2)	13.011(3)	13.011(3)	13.7952(18)	13.6662(11)	13.7952(18)	13.8927(5)
c (Å)	12.682(2)	12.766(3)	12.766(3)	15.095(3)	15.052(2)	15.095(3)	15.0744(11)
V(Å^3)	5675.3(17)	5809(2)	5809(2)	2872.7(8)	2811.3(6)	2872.7(8)	2909.5(3)
Z	4	4	4	2	2	2	2
d_{calc} (g·cm^{-3})	1.533	1.498	1.498	1.515	1.548	1.515	1.495
μ (mm^{-1})	0.609	0.595	0.595	0.601	0.614	0.601	0.594
T (K)	27(2)	200(2)	298(2)	33(2)	100(2)	213(2)	298(2)
R1[a] (wR2[b])	0.0595 (0.1272)	0.0390 (0.0823)	0.0441 (0.0848)	0.1222 (0.2218)	0.0983 (0.2062)	0.0719 (0.1649)	0.0541 (0.1408)

[a] $R1 = [\Sigma w(F_o-F_c)^2/\Sigma wF_o^2]^{1/2}$. [b] $wR2 = [\Sigma w(F_o^2-F_c)^2/\Sigma w(F_o^2)^2]^{1/2}$, $w = 1/[\sigma^2(F_o^2)+(aP)^2+bP]$, *where* $P = [\max(F_o^2,0)+2(F_c^2)]/3$.

4. Conclusions

The isolation of a pair of diruthenium compounds having the same core but very different axial interactions has allowed us to obtain important insight into the electronic structures of Ru_2^{5+} cores. These compounds show that there is a significant impact of metal-ligand π interactions in the electronic structure of metal systems that is responsible for changes in various physical properties. Specifically, the removal of axial interactions in Ru_2^{5+} systems allows for the manipulation of the magnetism. DFT calculations support the ground states observed by magnetic measurements, and confirm the qualitative MO picture predicted by MO theory. The magnetic and structural data is consistent with the existence of combined ligand σ/metal σ and ligand pπ/metal-dπ interactions. The confirmation and isolation of this type of interactions may lead to significant advances in the control of magnetic behavior.

Chapter 3: Stabilization of a W_2^{6+} Bimetallic Complex Supported by Two N,N',N''-Triphenylguanidinate Ligands[‡]

1. Introduction

The discovery 50 years ago of the first quadruply bonded complex, $[Re_2Cl_8]^{2-}$, created a paradigm shift in the field of inorganic chemistry. Since then, hundreds of bimetallic complexes with different bond orders and electronic properties have been synthesized and structurally characterized.[1,54,55] The understanding of the electronic and bonding properties of $[Re_2Cl_8]^{2-}$, according to molecular orbital theory, has led to the rational design of inorganic complexes. Beyond the practical applications of bimetallic complexes,[4-6] the electronic composition and manipulation of metal units at the molecular level is still a main area of research. The electronic configuration of group six transition metal elements is suitable to the formation of bimetallic complexes with a bond order of four. Thus, the chemistry of dichromium and dimolybdenum (Cr_2, Mo_2) complexes is very rich spanning oxidation states of 4+, 5+, or 6+ and hundreds of different complexes.[7,8] On the other hand, the chemistry of ditungsten (W_2) complexes is modest, in part, because of its more difficult synthetic pathways and their increased reactivity.

The syntheses of Cr_2 and Mo_2 complexes is easily accomplished by straight forward pathways utilizing simple salts or metal hexacarbonyls as starting materials, (Equation 1 and 2). Yet, the synthesis of W_2 complexes requires, for the most part, a multi-step process where WCl_4 is reduced to form the thermally unstable $[W_2Cl_8]^{4-}$ anion (Equation 3).[7,9-11]

(1) $2CrCl_2 + NaCOOCH_3 + 2H_2O \rightarrow Cr_2(O_2CCH_3)_4(H_2O)_2 + 4NaCl$

[‡] This chapter previously appeared as an article in Inorganica Chimica Acta. The original citation is as follows: Ventura, K.; Veleta, M. J.; Metta-Magaña, A.; Villagrán, D.; Stabilization of a W_2^{6+} bimetallic complex supported by two *N,N',N''*-triphenylguanidinate ligands. *Inorg. Chim. Acta* ,**2015**, *424*, pp.286-292

(2) $2Mo(CO)_6 + 4HCOOCH_3 \rightarrow Mo_2(O_2CCH_3)_4 + 2H_2 + 12CO$

(3) $2WCl_4 + 4KC_8 \rightarrow 4K^+ + [W_2Cl_8]^{4-} + Li[Ligand] \rightarrow W_2(Ligand)_4 + 4LiCl + 4KCl$

Carboxylates, formamidinates, and guanidinates have been successful ligands used to synthesize bimetallics complexes.[12,13] Among them, guanidinates have been the focus of interest due to their high basicity which allows them to stabilize M_2 units with high oxidation states.[14-19] For instance, group six bimetallic units bridged by 1,3,4,6,7,8-hexahydro-*2H*-pyrimido[1,2-a]pyrimidine (hpp) have been found to have very low ionization energies, and the W_2 analog shows an ionization energy of 3.51 eV which is lower than that for the cesium atom (3.89 eV).[19] A recent report using alkylated versions of the hpp ligands improved the solubility of W_2^{n+} (n = 6, 4) complexes in organic solvents, and further lowered the ionization energy of these complexes.[20] Recently, a direct way to synthesize W_2 compounds starting from $W(CO)_6$ has been found using a high boiling point solvent, such as *o*-dichlorobenze, but the thermal stability of the ligand has to be high.[21,22]

Another difference among group six M_2 complexes is the richness of the chemistry of the Mo_2 compared to W_2 towards supramolecular chemistry. In contrast to Mo_2,[22-32] there are very few mixed-ligand W_2 precursors that can be used towards the building of higher order systems, such as dimer of dimers.[33,11]

In this study we present the synthesis and characterization of a less common dimetal complex with a D_{2h} core and a W–W triple bond, where *N,N',N''*-triphenylguanidinate (TPG) ligands are *trans* to each other while chloride ligands occupy the equatorial plane of the molecule, $W_2(TPG)_2Cl_4$, **1**. We have probed the reduction chemistry of this compound through electrochemical measurements by the reaction of **1** with KC_8 to yield a complex with a bond

order of 3.5, **2**. Density Functional Theory (DFT) studies have been performed in order to understand the electronic structure of **1**, and the nature to its multiple bonding character. We propose that this complex can be used as a precursor towards the synthesis of well-defined W_2 supramolecular assemblies such as the ones depicted in Scheme 3.1 where bimetallic units are bridged to one another by bisbidentate ligands

2. Experimental

2.1. General Synthetic Procedures

Standard vacuum line, dry-box, and Schlenk techniques under nitrogen atmosphere were employed for the synthesis of all compounds. All solvents were dried and degassed using a Pure Process Technology solvent purification system prior to use. Tungsten tetrachloride was synthesized according to previously reported literature procedures.[10] *N,N',N''*-Triphenyl guanidine (HTPG) was purchased from TCI America and used without any further purification.

2.2. Physical Measurements

The UV-Vis spectrum for $W_2(TPG)_2Cl_4$ in THF was recorded on a SEC2000 spectra system equipped with visual spectra 2.1 software from 200 to 800 nm. ^{1}H NMR spectrum was recorded in a 5 mm NMR tube on a JEOL 600 MHz NMR spectrometer. The proton chemical shifts (δ) of $W_2(TPG)_2Cl_4$ were referenced to the residual $(CH_3)_2SO$ (δ = 2.50) in $(CD_3)_2SO$ solvent. FT-IR

Scheme 3.1 Tungsten bimetallic units as building blocks of supramolecular chemistry

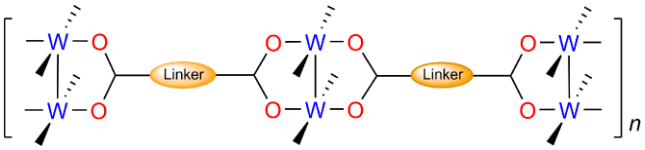

Spectrum was recorded on a Perkin-Elmer Spectrum 100 FT-IR Spectrometer from 4000 to 650 cm^{-1}. Raman Spectrum was recorded on a Thermo Scientific^{TM} DXR SmartRaman spectrometer

using a 532 cm^{-1} filter. Electrochemical analysis was performed in THF using a CHI760D potentiostat with a 2 mm diameter Pt working electrode, Pt mesh auxiliary electrodes and Ag/Ag^{+} (AgCl) reference electrode. The Pt working electrode was polished with a Buehler alumina micropolish kit immediately before the experiment. Measurements were conducted at a scan rate of 0.1 V/s on a 10 mL THF solution containing 1 mM of sample **1** and 0.1 M of tetrabutylammonium hexaflourophosphate. Voltammograms were internally referenced to

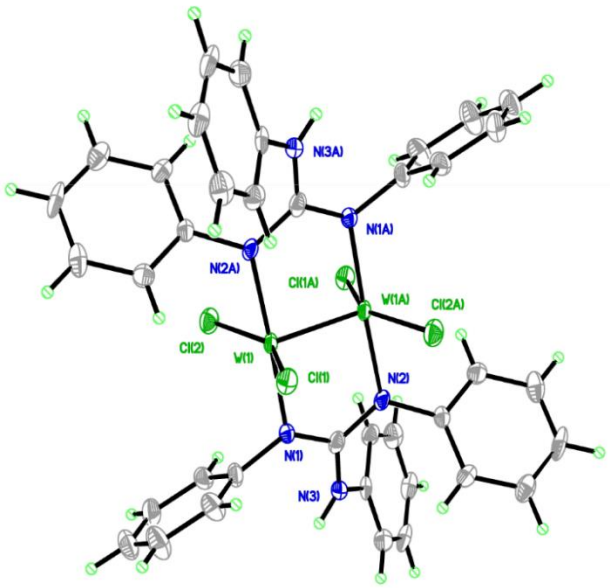

Figure 3.1 Crystal structure of **1** at 100 K. Drawn with displacement ellipsoids at the 50% probability level.

$FeCp_2/FeCp_2^{+}$. The X-band (~ 9.5 GHz) EPR spectrum was obtained using a BrukerEMXplus spectrometer with an ER073 magnet. To increase solubility of **2** in toluene, two drops of THF were added to 2 mL of EPR sample. Mass spectrum of **1** was obtained using a Bruker microFlex MALDI–TOF spectrometer on reflector positive mode using 1,1,4,4–tetraphenyl–1,3–butadiene as matrix. All samples were measured at room temperature.

Table 3.1. Crystallographic data for **1**

Compound	**1**
Formula	$C_{38}\ H_{32}\ Cl_4\ N_6\ W_2$, $2(C_4\ H_8\ O)$
Crystal system	Triclinic
Space group	$P\bar{1}$
a (Å)	9.8861(7)
b (Å)	10.9531(7)
c (Å)	11.5383(8)
α (deg)	111.677(1)
β (deg)	94.412(1)
γ (deg)	97.646(1)
V (Å^3)	1139.9(1)
Z	1
d_{calc} (g·cm^{-1})	1.787
μ (mm^{-1})	5.321
2*Θ* range, deg	3.83– 60.0
λ, Å	0.71073
T, °C	–173
GOF	0.973
R1,[a] wR2[b] ($I > 2\sigma(I)$)	0.0401, 0.0762

[a] $R1 = \Sigma||F_o| - |F_c||/ \Sigma|F_o|$. [b] $wR2 = [\Sigma[w(F_o^2 - F_c^2)^2]/ \Sigma w(F_o^2)^2]^{1/2}$, w = $1/[\sigma^2(F_o^2) + (aP)^2 + bP]$, where $P = [\max(F_o^2 \text{ or } 0) + 2(F_c^2)]/3$

2.3. X-ray Crystallography

A single crystal of approximately 0.09 x 0.05 x 0.03 mm^3 dimensions was mounted on a glass fiber using silicon grease. The x-ray intensity data were measured on a Bruker SMART APEX CCD system equipped with a graphite monochromator and a MoKα fine-focus tube (λ = 0.71073 Å).

The frames were integrated with the Bruker SAINT software package using a narrow-frame algorithm. The integration of the data using a triclinic unit cell yielded a total of 203251 reflections to a maximum *θ* angle of 30.00° (0.71 Å resolution), of which 6604 (with an average redundancy of 3.360) were independent and of which 5406 were greater than $2\sigma(F^2)$. (Data completeness = 100.0%, Rint = 4.34%, Rsig = 4.60%) The final unit cell dimensions of a = 9.8861(7) Å, b = 10.9531(7) Å, c = 11.5383(8)Å, α = 111.677(1)°, β = 94.412(1)°, γ = 97.646(1)°, volume = 1139.9(1)Å^3, are based upon the refinement of the xyz-centroids of reflections above 20 $\sigma(I)$. Data were corrected for absorption effects using the multi-scan method

(SADABS). The calculated minimum and maximum transmission coefficients (based on crystal size) are 0.5900 and 0.7463.

The structure was solved and refined by direct methods using the Bruker SHELXTL Software Package, using the space group $P\bar{1}$, with Z = 1 for compound **1**. The final anisotropic full-matrix least-squares refinement on F^2 with 275 variables converged at R_1 = 4.01%, for the observed data and wR_2 = 7.62% for all data. The goodness-of-fit was 0.973. The largest peak in the final difference electron density synthesis was 1.698 $e^-/Å^3$ and the largest hole was –1.661 $e^-/Å^3$ with an RMS deviation of 0.216 $e^-/Å^3$. On the basis of the final model, the calculated density was 1.787 g/cm^3 and $F(000)$, 598 e^-.

Table 3.2 Calculated and experimental data from compounds **1** and **2**

Compound	Atoms	Calculated Distance (Å)	Experimental Distance (Å)	Total Energy (Hartrees)	Experimental Raman (cm-1)	Calculated Raman (cm-1)
1	W(1)-W(1A)	2.28	2.2604(4)	-3772.5796965	290	296
	W(1)-N(1)	2.11	2.072(4)			
	W(1)-N(2A)	2.12	2.083(4)			
	W(1)-Cl(1)	2.38	2.333(1)			
	W(1) - Cl(2)	2.36	2.339(1)			
2	W(1)-W(1A)	2.26		-3772.6646711	315	332
	W(1)-N(1)	2.14				
	W(1)-N(2A)	2.14				
	W(1)-Cl(1)	2.43				
	W(1) - Cl(2)	2.41				

2.4. Computational Details

Density Functional Theory (DFT)[34,35] calculations were performed with the hybrid Becke-3 parameter exchange functional[36,38] and the Lee-Yang-Parr nonlocal correlation functional[39] (B3LYP) implemented in the Gaussian 09[40] (Revision C.01) program suit. Double-ζ-quality basis sets (D95) were used on nonmetal atoms (carbon, nitrogen and hydrogen). An effective core potential (ECP) representing the 1s2s2p3s3p3d core was used for the tungsten atoms along

with the associated double-ζ basis set (LANL2DZ). The convergence criterion for the self-consistent field cycles on all calculations was increased from the default value to 10^{-8}. All the calculations were performed on a full-atom model of **1** and **2** with no simplifications. Geometry optimization calculations were found to be minima in the potential energy surface as evidenced by the lack of imaginary vibrations in the frequency calculations. Polarizability derivatives (Raman intensities) were computed using the Gaussian 09 package using the keywork freq=Raman. All calculations were performed in a 44-processor PowerWolf PSSC supercomputer cluster running Linux Red Hat 4.1.2-54 located at the University of Texas at El Paso.

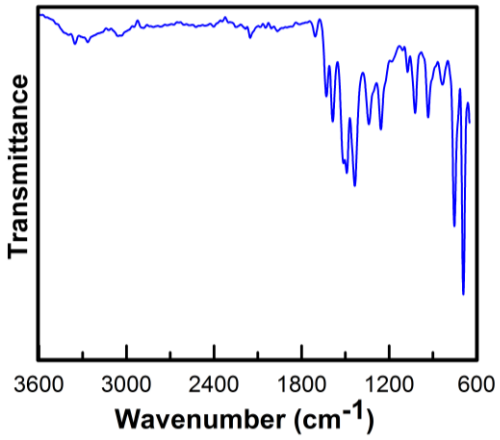

Figure 3.2 FT-Infrared Spectrum of **1**

2.5. Syntheses

2.5.1. $W_2(TPG)_2Cl_4$ (1)

WCl_4 (0.500 g, 1.5 mmol) was reacted with KC_8 (0.208 g, 1.5 mmol) in 30 mL of THF at –94˚C (liquid N_2 and acetone bath) under N_2 atmosphere until deep green coloration was observed. In a separate flask, LiTPG was prepared by reacting HTPG (0.441g, 1.5mmol) and methyllithium

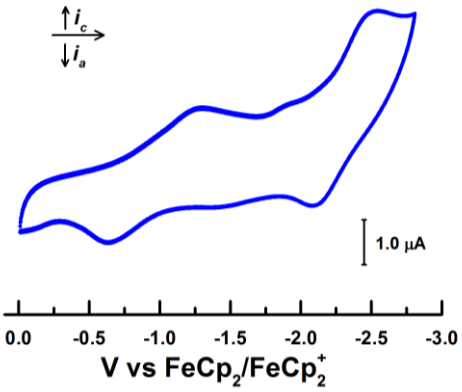

Figure 3.3 Cyclic Voltammogram in THF of **1**

(1.05mL, 1.68mmol) in 10 mL of THF at 0˚C. The lithium guanidinate salt, that formed upon warming the solution to r.t., was slowly added with a double tipped needle (canula), for a period of 2 min, to the reduced ditungsten solution. The color turned redish-brown after c.a. 1.5 h then the solution was filtered with a medium coarse filter. The solvent was removed under reduced pressure. The obtained solid was washed thoroughly with diethyl ether and hexanes, and dried under reduced pressure. Brown-yellow crystals appeared within 2 days by THF/Hexanes layer diffusion. Isolated yield 0.700g, 43%. UV-Vis (THF): 264 nm (sh), ^{1}H NMR spectroscopy ($(CD_3)_2SO$): δ 7.16 (m, 6H, aromatic C-H), 7.29 (m, 12H, aromatic C-H), 7.34 (m, 12H, aromatic C-H), 10.71 (s, 2H, -CNHC-). MALDI–TOF MS: calcd. 1081.05 $[M + H]^+$, found 1081.33 $[M + H]^+$. CV (V vs. $FeCp_2/FeCp_2^+$): E'ap:–1.28, E'cp: –0.63, $E'_{1/2}$: –0.95, E"ap: – 2.52,

E”cp: – 2.10, E”1/2: – 2.31. IR (cm^{-1}): v = 3352, 3064, 1709, 1630, 1486, 1437, 1341, 1258, 1020, 932, 829, 754, and 690. Raman (cm^{-1}): v = 290.

2.5.2. Synthesis of $W_2(TPG)_2Cl_4K$ (2)

A mixture of 0.100 g (0.092 mmol) of 1 and 0.012 g (0.092 mmol) of KC_8 was cooled down to – 94˚C and 20 mL of THF was slowly added. The reaction was allowed to warm up to room temperature, and then it was filtered with a medium coarse fritted disk. Volatiles were removed under reduced pressure. UV-Vis (THF): 295 nm (sh). IR (cm^{-1}): v = 2962, 1684, 1595, 1534, 1487, 1442, 1311, 1257, 1229, 1019, 799, 749, and 689. EPR: g = 1.83. Raman (cm^{-1}): v = 315.

3. Results and Discussion

The reaction between WCl_4, KC_8 and LiTPG in THF resulted in a microcrystalline powder of $W_2(TPG)_2Cl_4$. Compound **1** is moisture sensitive and soluble in donor solvents, such as THF, and partially soluble in aromatic solvents, such as benzene. Reactivity with chlorinated solvents such as DCM and chloroform was observed.

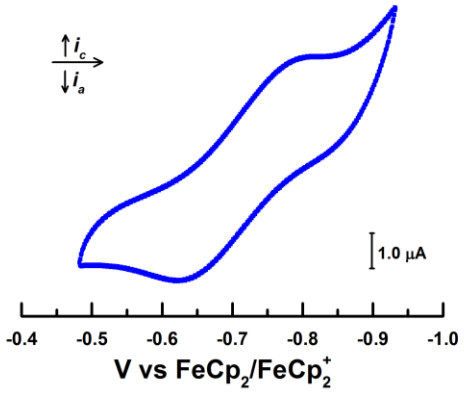

Figure 3.4 Cyclic voltammogram showing the first reversible redox event of **1.**

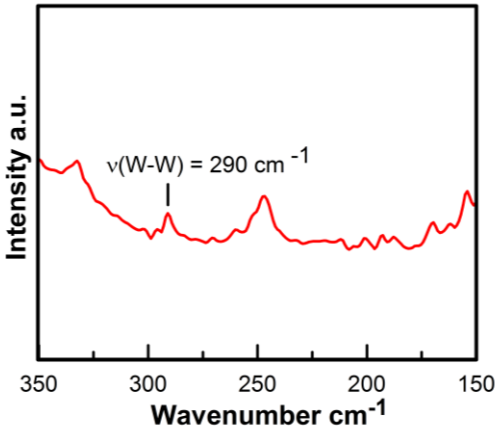

Figure 3.5 Raman spectrum of **1.**

Crystals grown from THF/hexane layer diffusion, at room temperature, were analyzed through single-crystal x-ray diffraction. The structure of **1** is shown in Figure 3.1. Relevant cell parameters, bond lengths and angles are presented in Tables 3.1 and 3.2. The W–W bond length in **1**, 2.2604(4) Å, is among the shortest triply bonded W_2 compounds (spanning between 2.236 and 2.375 Å).[41,42] A recently reported edge-sharing bioctahedral W_2 complex, $[W_2(\mu\text{-O})(\mu\text{-TMhpp})Cl_2]_2^{2-}$, where TMhpp = 3,3,9,9-tetramethyl-1,5,7-triazabicyclo[4.4.0]dec-4-ene, with a

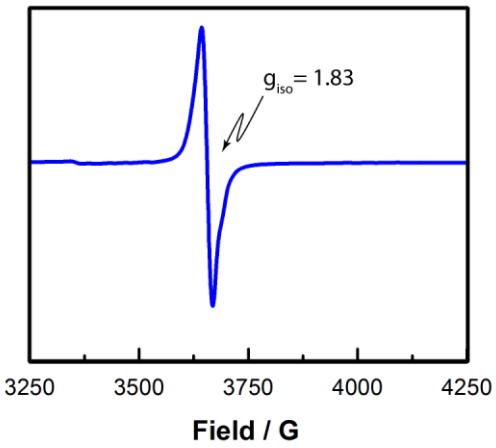

Figure 3.6 X-band EPR spectrum of **2.** Sample measured at room temperature in toluene solvent

W_2^{8+}core, was found to have a bond order of two and a much longer bond distance (2.3318 Å).[43]

The NMR spectrum of **1** shows multiplets at 7.16, 7.29, and 7.34 ppm assigned to the aromatic rings of the guanidinate ligand, and a singlet at 10.71 ppm which correspond to the N–H proton. The IR spectrum of **1** (Fig. 2) shows a well-defined band at 1258 cm^{-1}, assigned to the aromatic rings in the ligand. An N–H stretch at around 3352 cm^{-1} and an amine stretch at 1630 cm^{-1} are also observed.

The redox behavior of **1** was studied by cyclic voltammetry. Two one-electron reversible events are observed at ($E_{1/2}$) –0.95 V and –2.31 V (vs $FeCp_2/FeCp_2^+$), and shown in Figures 3.3 and 3.4.

This suggests that the one and two electron reduction products should be synthetically accessible. Therefore, reduction of **1** with one equivalent of KC_8 in THF results in a complex with bond order of 3.5 (**2**).[43] Compound **2** is moisture and air sensitive, with the same solubility and reactivity towards chlorinated solvents as its precursor. A weak event is observed at ($E_{1/2}$) –1.67 V due to small traces of oxygen in the electrochemical cell which readily reacts with the doubly reduced species (**2**). Isolation of the first redox wave (Figure 3.4) shows a reversible one-eletron redox wave with no signs of sample decomposition. The NMR spectrum of **2** exhibits broad signals suggesting a paramagnetic compound. Furthermore, the IR spectrum of **2** is similar to that of **1**, with the signals showing a hypsochromic shift compared to the precursor. Raman spectroscopy was used to further study tungsten-tungsten vibronic interactions in the metal centers for **1** and **2** and to compare the relative strength of the W–W vibration between the neutral specie and its anion. The spectra were recorded with an excitation of 532 nm and the spectrum for **1** is shown in Figure 3.5. The *v* (W–W) Raman shift for **1** is shown at 290 cm^{-1} and falls within the range of triply bonded W_2 complexes (280-300 cm^{-1}).[44] Reduction of **1** to **2** shifts the *v* (W–W) Raman signal to 315 cm^{-1}, consistent with the higher bond order in the

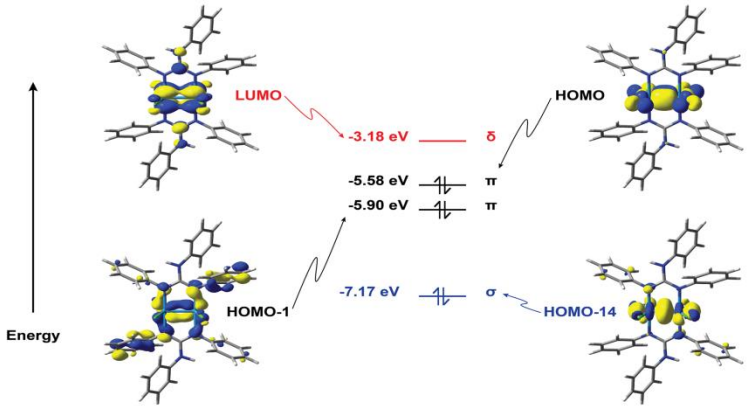

Figure 3.7 Illustration of the 0.04 contour surface diagrams of three highest occupied and one lowest unnocupied MOs calculated by DFT for **1**.

reduced complex. The Raman shift for the reduced complex is comparable to quadruply bonded W_2 systems.[45] This is explained by the high electron donating properties of the guanidinate ligand. Signals below 300 cm^{-1} were difficult to assign due to the large amount of scattering from the sample and glass vial.[46] DFT calculations based on full models of **1** and **2** show the *v* (W–W) Raman shifts at 296 cm^{-1} and 332 cm^{-1}, respectively. The calculated difference in Raman shifts between **1** and **2** is of 36 cm^{-1} which is comparable with the experimental shift of 25 cm^{-1}.

Since **2** is expected to have one unpaired electron and a ground state of S = ½, its electronic properties were probed by EPR spectroscopy in toluene solution at RT (Figure 3.6). The spectrum shows an isotropic signal with g = 1.83. The EPR signal is broad due to electron coupling to the 14% abundant ^{183}W nuclei (S = ½), but we were not able to resolve the doublet satellites at the measured X-band and at RT.

Density Functional Theory (DFT) calculations on full-atom models of **1** and the anion in **2** were

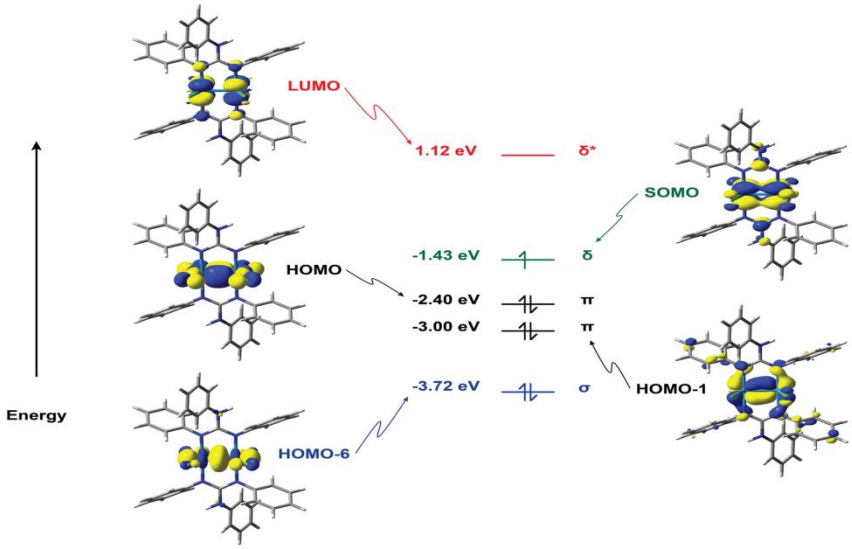

Figure 3.8 Illustration of the 0.04 contour surface diagrams of three highest occupied, singly occupied, and lowest occupied MOs calculated by DFT for **2**

performed in order to obtain information about the electronic structure of the W_2 core. The crystallographic information was used as the starting point for the geometry optimizations of **1**, and the resulting geometry was used as the starting point for the unrestricted open-shell calculation of the anion of **2**. Selected geometrical data and thermodynamic data are shown in Table 3.2. The calculated W–W bond distance in the model of **1** is 2.28 Å and it is comparable to the experimentally observed 2.2604(4)) Å. The calculated W–W bond distance for the model of the anion of **2** is 2.26 Å, which is consistent with the strengthening of the W–W bond going from 3 to 3.5 in **1** and **2**, respectively.

The electronic structure for the model of **1** shows that the HOMO (–5.58 eV) is metal based with π character (Figure 3.7). The HOMO–1 is the second orthogonal π orbital at about 0.32 eV lower in energy. HOMO–1 also shows some strong ligand interaction between the N atoms from TPG and the metal center which further confirm the strong interaction between the guanidinate ligand and the W_2 core. In contrast to D_{4h} paddlewheel complexes, the two π orbitals are not degenerate due to the different interactions between the Cl and TPG ligands. The metal based σ orbital is very stable and found at HOMO–14 (–7.17 eV). The LUMO of **1** is the metal based δ orbital found at –3.18 eV. The open shell calculation for the model of **2** shows that the SOMO (Figure 3.8) is the metal based δ orbital. This is expected from the standard MO diagram for tetragonal complexes.

4. Conclusion

A triply bonded $W_2(TPG)_2Cl_4$ was prepared and structurally characterized. The one electron reduction product of **1** was analyzed by EPR and Raman spectroscopies. Data from Raman spectroscopy shows an increase in the ν(W–W) Raman shift from **1** to **2** consistent with the

increase in bond order from 3 to 3.5, respectively. DFT calculations depict strong interaction between the metal and guanidine ligand orbitals, and support our Raman assignments and metal-based MO picture. We expect compound **1** to serve as a precursor for the synthesis of W_2 supramolecular assemblies similar to those reported with Mo_2 metal centers and to those obtained with W_2 supported by carboxylate ligands.[47]

Chapter 4: Conclusion

Four ruthenium complexes, $Ru_2(Dani^mF)_4Cl$, $Ru_2(Dani^pF)_4Cl$, $Ru_2(Dani^mF)_4BF_4$ and $Ru_2(Dani^pF)BF_4$, with an idealized D_{4h} symmetry were successfully synthesized. Their structural, magnetic and electronic characterization demonstrated the importance of π metal-ligands interactions in the electronic structure in bimetallic systems containing a Ru_2^{5+} core and their role in manipulating the magnetism of these types of complexes. On those containing a chloride as an axial ligand two possible ground states can be found: two electrons in the π* orbitals and one in the δ* orbitals, or three electrons in the π* orbitals. For the complexes containing a non-coordinative axial ligand, a ground state, consisting of three electrons in the π* orbitals was observed at all times. EPR data successfully confirmed that the observed unpaired electrons reside in metal-based molecular orbitals. DFT calculations also support all of the ground states observed. Based on the magnetic data presented it can be concluded that the isolation of combined ligand *σ*/ metal *σ* and ligand *pπ* / metal *pπ* interactions can control the magnetic behavior of these complexes.

In order to explore D_{2h} complexes with a bond order of three, a tungsten compound, $W_2(TPG)_2Cl_4$, was successfully synthesized and structurally characterized. Single-crystal x-ray crystallography showed a W-W bond distance of 2.2604(4) Å which is among the shortest triple bonds between W_2 compounds reported. Cyclic voltammetry showed two one-electron reversible redox events demonstrating the possibility of synthesizing two compounds, one with a bond order of 3.5 and the other with a bond order of 4 respectively. The reduction of $W_2(TPG)_2Cl_4$ with one equivalent of KC_8 results in a complex with a bond order of 3.5. The anion, obtained by a one electron reduction of the parent compound, was carefully studied by EPR demonstrating that the unpaired electron resides in a metal-based orbital. DFT calculations show that the

unpaired electron resides in an orbital of delta symmetry. DFT calculations were also used to assign the experimentally obtained Raman spectra. The calculated Raman spectra shows that there is a shift of 36 cm^{-1} between the neutral and reduced complexes consistent to those observed experimentally of 25 cm^{-1}.

Even though the chemistry of bimetallic complexes has been a focus of intense research, there is still a wide range of factors that still need to be understood, for example, the exploration of highly unsaturated bimetallic centers, with a bond order of five, as well as the use of these complexes for the reductive elimination of small molecules.[5] By comprehending the magnetic and electronic properties of different symmetries and different transition metals, we are one step closer to fully apprehend the nature of metal-metal bonds. It is also important to notice that ligands perform an important role in the bonding between metals, and they also help manipulate the magnetic properties of the mentioned metal-metal bonds. Exploration of one and two dimensional supramolecular complexes containing bimetallic units is yet to be explored, as well as their use for the synthesis of Metal-organic Frameworks (MOFs). More importantly understanding the electronic structure of ditungsten units, has given us insight to develop a series of D_{2h} complexes supported by different guanidinates and formamidinates ligands with a great potential to form bimetallic systems with a high bond order.

References

(1)Cotton, F. A.; Curtis, N. F.; Harris, C.B.; Johnson, B.F. G.; Lippard, S. J.; Mague, J. T.; Robinson, W. R.; Wood, J. S. *Science* **1964**, 145, 1305

(2)Cotton, F. A.; Murillo, C. A.; Walton, R. A., Eds. *Multiple Bonds between Metal Atoms*, 3rd ed.; Springer Science and Business Media, Inc.; New York, **2005**.

(3)Shen J.; Yap G. P. A.; Theopold K. H. *Chem. Commun.* **2014**, 50, 2579

(4)Noor, A.; Kempe R. *Inorg. Chim. Acta.* **2015**, 424, 75

(5)Nair, A. K.; Harisomayajula S.; Tsai, Y. C. *Dalton Trans*, **2014**, 43, 5618

(6) For example, see: (a) Chisholm, M. H., Ed. *Early Transition Metal Clusters with pi-Donor Ligands*, VCH: New York, 1995. (b) Shriver, D. F.; Kaesz, H. D.; Adams, R. D., Eds. *The Chemistry of Metal Cluster Complexes*, VCH: New York, 1990. (c) Cotton, F. A.; Wilkinson, G.; Murillo, C. A.; Bochmann, M. *Advanced Inorganic Chemistry*, Wiley: New York, 1999. (d) Vogeley, N. J.; Templeton, J. L. *Polyhedron* 2004, 23, 311. (e) D'Souza, F.; Ito, O. *Chem. Commun*. **2009**, 4913. (f) Schneider, H.-J. *Angew. Chem., Int. Ed.* **2009**, 48, 3924. (g) Vignolle, J.; Cattoen, X.; Bourissou, D. *Chem. Rev*. **2009**, *109*, 3333. (h) Bellachioma, G.; Ciancaleoni, G.; Zuccaccia, C.; Zuccaccia, D.; Macchioni, A. *Coord. Chem. Rev*. **2008**, *252*, 2224. (i) Holland, P. L. *Acc. Chem. Res*. **2008**, *41*, 905. (j) Hay, B. P.; Bryantsev, V. S. *Chem. Commun*. **2008**, 2417. (k) Schottel, B. L.; Chifotides, Helen T.; Dunbar, Kim R. *Chem. Soc. Rev*. **2008**, *37*, 68. (l) Hembury, G. A.; Borovkov, V. V.; Inoue, Y. *Chem. Soc. Rev*. **2008**, *37*, 1. (m) Petrukhina, M. A. *Coord. Chem. Rev*. **2007**, *251*, 1690. (n) Gamez, P.; Mooibroek, T. J.; Teat, S. J.; Reedijk, J. *Acc. Chem. Res*. **2007**, *40*, 435. (o) Chisholm, M. H. *Proc. Nat. Acad. Sci. U.S.A.* **2007**, *104*, 2563. (p) Conradie, J.; Tangen, E.; Ghosh, A. *J. Inorg. Biochem*. **2006**, *100*, 707. (q) Omary, M. A.; Mohamed, A. A.; Rawashdeh-Omary, M. A.; Fackler, Jr., J. P. *Coord. Chem. Rev*. **2005**, *249*, 1372. (r) Sakaki, S.; Biswas, B.; Musashi, Y.; Sugimoto, M. *J. Organomet. Chem*. **2000**, *611*, 288.

(7) (a) Cotton, F. A.; Murillo, C. A.; Reibenspies, J. H.; Wang, X.; Wilkinson, C. C. *Inorg. Chem.* **2004**, *43*, 8373. (b) Angaridis, P.; Cotton, F. A.; Murillo, C. A.; Villagrán, D.; Wang, X. *J. Am. Chem. Soc*. **2005**, *127*, 5008.

(8) (a) Stephenson, T. A.; Wilkinson, G. *J. Inorg. Nucl. Chem*. **1966**, *28*, 2285. (b) Bennettt, M. J.; Caulton, K. G.; Cotton, F. A. *Inorg. Chem*. **1969**, *8*, 1.

(9) Norman, J. G.; Renzoni, G. E.; Case, D. A. *J. Am. Chem. Soc*. **1979**, *101*, 5256.

(10) Angaridis, P. in Cotton, F. A.; Murillo, C. A.; Walton, R. A. Eds. *Multiple Bonds between Metal Atoms*, Springer Science and Business Media, Inc., New York, 2005, Ch. 9.(6) (a) Aquino, M. A. S. *Coord. Chem. Rev*. **2004**, *248*, 1025. (b) Aquino, M. A. S. *Coord. Chem. Rev*. **1998**, *170*, 141. (c) Bear, J. L.; Han, B.; Huang, S.; Kadish, K. M. *Inorg. Chem*. **1996**, *35*, 3012. (d) Chiarella, G. M.; Cotton, F. A.; Murillo, C. A.; Young, M. D.; Zhao, Q. *Inorg. Chem.* **2010**, *49*, 3051. (e) Lee, R.; Yang, Y. Y.; Tan, G. K.; Tan, C.-H.; Wang, K.-W. *Dalton Trans*. **2010**, *39*, 723. (f) Pap, J. S.; Snyder, J. L.; Piccoli, P. M. B.; Berry, J. F. *Inorg. Chem*. **2009**, *48*, 9846. (g) Pap, J. S.; DeBeer George, S.; Berry, J. F. *Angew. Chem. Int. Ed*. **2008**, *47*, 10102. (h) Cummings, S. P.; Savchenko, J.; Fanwick, P. E. Kharlamova, A, Ren T. *Organometallics* **2013**, *32*, 1129. (i) Savchenko, J.; Fanwick, P. E.; Hope, H.; Gao, Y.; Yerneni, C. K.

Ren, T. *Inorg. Chim. Acta* **2013**, *396*, 144. (j) Boudreau, L. J.; Clarke, T. L.; Murray, A. H.; Robertson, K. N.; Cameron, T. S.; Aquino, M. A. S. *Inorg. Chim. Acta* **2013**, *394*, 152.

(11) See for example: (a) Telser, J.; Drago, R. S. *Inorg. Chem*. **1984**, *23*, 3114. (b) Cukiernik, F. D.; Luneau, D.; Marchon, J.-C.; Maldavi, P. *Inorg. Chem*. **1998**, *37*, 3698. (c) Jiménez-Aparicio, R.; Urbanos, F. A.; Arrieta, J. M. *Inorg. Chem*. **2001**, *40*, 613. (d) Handa, M.; Sayama, Y.; Mikuriya, M.; Nukuda, R.; Hiromitsu, I.; Kasuga, K. *Bull. Chem. Soc. Jpn*. **1995**, *68*, 1647. (e) Cheng, W.-Z.; Cotton, F. A.; Dalal, N. S.; Murillo, C. A.; Ramsey, C. M.; Ren, T.; Wang, X. *J. Am. Chem. Soc*. **2005**, *127*, 12691. (f) Liao, Y.; Shum, W. W.; Miller, J. S. *J. Am. Chem. Soc*. **2002**, *124*, 9336. (g) Barral, M. C.; Herrero, S.; Jiménez-Aparicio, R.; Torres, M. R.; Urbanos, F. A. *Angew. Chem., Int. Ed*. **2005**, *44*, 305. (h) Barral, M. C.; Gallo, T.; Herrero, S.; Jiménez-Aparicio, R.; Torres, M. R.; Urbanos, F. A. *Chem. Eur. J*. **2007**, *13*, 10088. (i) Miyasaka, H.; Motokawa, N.; Matsunaga, S.; Yamashita, M.; Sugimoto, K.; Mori, T.; Toyota, N.; Dunbar, K. *J. Am. Chem. Soc*. **2010**, *132*, 1532. (j) Barral, M. C.; González-Prieto, R.; Herrero, S.; Jiménez-Aparicio, R.; Priego, J. L.; Royer, E. C.; Torres, M. R.; Urbanos, F. A. *Polyhedron* **2004**, *23*, 2637. (k) Delgado, P.; Gonzalez-Prieto, R.; Jiménez-Aparicio, R.; Perles, J.; Priego, J.; Torress, R. M. *Dalton Trans*. **2012**, *41*, 11866. (l) Delgado-Martínez, P.; González-Prieto, R.; Gómez-García, C. J.; Jiménez-Aparicio, R.; Priego, J. L.; Torres, M. R. *Dalton Trans*. **2014**, *43*, 3227. (m) Haque, F.; del Barco, E.; Fishman, R. S.; Miller, J. S. *Polyhedron* **2013**, *64*, 73. (n) Da Silva, J. G.; Miller, J. S. *Inorg. Chem*. **2013**, *52*, 1418. (o) Her, J.-H.; Stephens, P. W.; Kennon, B, S.; Liu, C.; Miller, J. S. *Inorg. Chim. Acta* **2010**, *364*, 172. (p) Ikeue, T.; Kimura, Y.; Karino, K.; Iida, M.; Yamahi, T.; Hiromitsu, I.; Sugimori, T.; Yoshioka, D.; Mikuriya, M.; Handa, M. *Inorg. Chem. Commun*. **2013**, *33*, 133.

(12) For an account of electronic configurations in paddlewheel compounds, see Falvello, L. R.; Foxman, B. M.; Murillo, C. A. *Inorg. Chem*. **2014**, *53*, 9441

(13) The chemical composition of this system is $[Ru_2(OAc)(DPhF)_3(H_2O)](SO_3CF_3)\cdot THF$. In both paddlewheel molecules there is an axial water molecule that is hydrogen-bonded to a triflate anion but in only one of the Ru_2^{5+} species there is a hydrogen-bonded interaction between the water and the THF molecule. For the latter the Ru–Ru distances are 2.3637(6) Å at 30 K and 2.3255(5) Å at 298 K and for the molecule without devoid of hydrogen bonded interactions to the THF molecule these distances are 2.2950(6) Å and 2.3064(5) Å, respectively. See: Cotton, F. A.; Herrero, S.; Jiménez-Aparicio, R.; Murillo, C. A.; Urbanos, F. A.; Villagrán, D.; Wang, X. *J. Am. Chem. Soc*. **2007**, *129*, 12666.

(14) For references on non-coordinating anions, see for example: (a) Krossing, I.; Raabe, I. *Angew. Chem., Int. Ed*. **2004**, *43*, 2066 and references therein. (b) Rach, S. F.; Kühn, F. E. *Chem. Rev*. **2009**, *109*, 2061. (c) Adams, H.; Fenton, D. E.; McHugh, P. E.; Potter, T. J. Inorg. Chim. Acta **2002**, *331*, 117. (d) Sharma, R. P.; Singh, A.; Venugopalan, P.; Harrison, W. T. A. *J. Molec. Struct*. **2011**, *994*, 6. (e) Reisinger, A.; Trapp, N.; Knapp, C.; Himmel, D.; Breher, F.; Ruegger, H.; Krossing, I. *Chem. Eur. J*. **2009**, *15*, 9505. (f) Barriere, F.; Geiger, W. E. *J. Am. Chem. Soc*. **2006**, *128*, 3980.

(15) The use of a non-coordinating solvent is essential. Many compounds having Ru_2^{5+} cores with BF_4 or other non-coordinating counterions are known but without exception they contain axial ligands such as H_2O, acetonitrile and other coordinating neutral species. For example, see: (a) Bino, A.; Cotton, F. A.; Felthouse, T. R. *Inorg. Chem*. **1979**, *18*, 2599. (b) Cotton, F. A.; Lu, J.; Yokochi, *Inorg. Chim Acta* **1998**, *275-276*, 447. (c) Anez, E.; Herrero, S.; Jiménez-Aparicio, R.; Priego, J. L.; Torres, M. R.; Urbanos, F. A. *Polyhedron***2010**, *29*, 232. (d) Barral, M. C.; Herrero, S.; Jiménez-Aparicio, R.; Priego, J. L.; Torres, M. R.; Urbanos, F. A. *J. Mol. Struct*. **200**8, *890*, 221. (e) Barral, M. C.; Gallo, T.; Herrero, S.; Jiménez-Aparicio, R.; Torres, M. R.; Urbanos, F. A. *Chem. Eur. J*. **2007**, *13*, 10088. (f) Chisholm, M. H.; Christou, G.; Folting, K.; Huffman, J. C.; James, C. A.; Samuels, J. A.; Wesemann, J. L.; Wooddruff, W. H. *Inorg. Chem*. **1996**, *35*, 3643. (g) Furakawa, S.; Kitagawa, S. *Inorg. Chem*. **2004**, *43*, 6464.

(16) For additional information on substituents effects in dinuclear paddlewheel compounds and Hammett σ constants for DAniF species, see: Ren, T. *Coord. Chem. Rev*. **1998**, *175*, 43.

(17) For reference, the closest approach of a fluorine atom to a ruthenium atom is over 4.7 Å. The Ru(1)···F(3A) separation is 4.74(1), 4.75(1) and 5.04(2) Å at 200, 298 and 27 K, respectively.

(18) To our knowledge there is only one structure of a compound with an Ru_2^{5+} core that is devoid of axial ligands ($Ru_2(DPhF)_3Br_2$), but this is not a paddlewheel species. This compound has a dimetal core spanned by the bridging formamidinate bridges. The remaining equatorial positions are occupied by the two halide species. The Ru–Ru distance is 2.4011(4) Å and its magnetism is intermediate between that expected from either a species with three or one unpaired electron. See: Barral, M. C.; Gallo, T.; Herrero, S.; Jiménez-Aparicio, R.; Torres, M. R.; Urbanos, F. A. *Chem. Eur. J*. **2007**, *13*, 10088.

(19) Barral, M. C.; González-Prieto, R.; Jiménez-Aparicio, R.; Priego, J. L; Torres, M. R.; Urbanos, F. A. *Eur. J. Inorg. Chem*. **2003**, 2339 and references therein.

(16) The magnetic data for **2**, which is similar to that of diruthenium tetracarboxylates, show a highly anisotropic behavior with a strong ZFS, which can be modeled using the following set equations:

$$\chi_{|} = \frac{Ng_{\|}^2\beta^2}{kT}\frac{1 + 9\exp\left(-\frac{2D}{kT}\right)}{4\left[1 + \exp\left(-\frac{2D}{kT}\right)\right]}$$

$$\chi_{\perp} = \frac{Ng_{\|}^2\beta^2}{kT}\frac{4 + \left(\frac{3kT}{D}\right)\left[1 - \exp\left(-\frac{2D}{kT}\right)\right]}{4\left[1 + \exp\left(-\frac{2D}{kT}\right)\right]}$$

Where $\chi = (\chi_{\|} + 2\chi_{\perp})/3$, N is Avogadro's number, D is the ZFS parameter in cm^{-1}, β is the Bohr magneton, k is the Boltzmann constant, and T is the temperature in Kelvin. The modeling of the data of **2** with these equations yields anisotropic values of $g_{\|}$ and $g_{\perp}$ of 1.72(4) and 2.02(1), respectively, which are consistent with the EPR data (vide supra), and the value of D of 75(3) is consistent to that of similar diruthenium complexes.

(20) The crystal structure of **1** has interstitial CH_2Cl_2 with an occupancy of 0.5, which plays no role in itrs structure since it resides in a noncoordinating position away from the axial location.

(21) Kondo, M.; Hamatami, M.; Kitagawa, S. *J. Am. Chem. Soc*. **1998**, *120*, 455.

(22) For large values of D and $S = {}^3/_2$, the effective (g^e) and actual g-values are related by $g_{\perp} = g_{\perp}^e/2$ and $g_{\|} = g_{\|}^e$. See ref **Error! Bookmark not defined.**e or Pilbrow, J. R. *J. Mag. Res*. **1978**, *31*, 479. In addition $_{iso} = (2g_{\perp} + g_{\|})/3$

(23) *Multiple Bonds between Metal Atoms*; Cotton, F. A.; Murillo, C. A.; Walton, R. A. Eds.; Springer Science and Business Media, Inc.: New York, 2005.

(24) Cotton, F. A.; Hillard, E. A.; Murillo, C. A.; Zhou, H-C.*J. Am. Chem. Soc*. **2000**, *122*, 416.

(25) Cotton, F. A.; Hillard, E. A.; Liu, C. Y.; Murillo, C. A.; Wang, W.; Wang, X. *Inorg. Chim. Acta* **2002**, *337*, 233.

(26) Cotton, F. A.; Hillard, E. A.; Murillo, C. A. *J. Am. Chem. Soc.* **2002**, *124*, 5658.

(27) Cotton, F. A.; Daniels, L. M.; Murillo, C. A.; Pascal, I.; Zhou, H.-C.*J. Am. Chem. Soc*. **1999**, *121*, 6856.

(28) Cotton, F. A.; Donahue,J. P.; Lichtenberger,D. L.; Murillo,C. A.; Villagrán, D.*J. Am. Chem. Soc*. **2005**, *127*, 10808.

(29) Cotton, F. A.; Donahue, J. P.; Gruhn, N. E.; Lichtenberger, D. L.; Murillo, C. A.; Timmons, D. J.; Van Dorn, L. O.; Villagrán, D.; Wang, X. *Inorg*. *Chem*. **2006**, *45*, 201.

(30) Chiarella, G. M.; Cotton, F. A.; Murillo, C. A.; Young, M. D. *Inorg. Chem*. **2011**, *50*, 1258.

(31) Barral, M. C.; Herrero, S.; Jiménez-Aparicio, R.; Torres, M. R.; Urbanos, F. A. *Inorg. Chem. Commun*. **2004**, *7*, 42.

(32) Angaridis, P.; Cotton, F. A.; Murillo, C. A.; Wang, X. *Acta Crystallogr*. **2005**, *C61*, m71.

(33) Barral, M. C.; Casanova, D.; Herrero, S.; Jiménez-Aparicio, R.; Torres, M. R.; Urbanos, F. A. *Chem. Eur*. *J*. **2010**, *16*, 6203.

(34) See for example: Liu, I. P.-C.; Ren, T. *Inorg. Chem.* **2009**, *48*, 5608.

(35) Even though the calculated absolute value may not fully agree, the trend (see text) is relevant.

(36) Note that the σ and σ* orbitals also drop in energy because of the symmetry-allowed σ-L interaction, but this drop in energy does not affect the overall multiplicity of the systems as the π interaction does.

(37) The calculated Ru-Ru distances according to the DFT optimized models closely resemble the experimentally observed bond distances. The calculated Ru-Ru bond distance for the doublet model without and axial ligand is 2.4138(5) Å, which is similar than those of **1**, 2.3968(5) and **2**, 2.3398(4) Å.

(38) (a) Cotton, F. A.; Daniels, L. M.; Murillo, C. A.; Schooler, P. *Dalton Trans*. **2000**, 2007. (b) Mohamed, A. A.; Abdou, H. E.; Irwin, M. D.; López-de-Luzuriaga, J. M.; Fackler, Jr., J. P. *J. Clust. Sci*. **2003**, *14*, 253.

(39) Mitchell, R. W.; Spencer, A.; Wilkinson, G. *J. Chem. Soc., Dalton Trans.* **1973**, 846.

(40) Angaridis, P.; Cotton, F. A.; Murillo C. A.; Villagrán, D.; Wang, X. *Inorg. Chem.* **2004,** *43*, 8290-8300.

(41) *Theory and Applications of Molecular Paramagnetism*, Boudreaux, E. A.; Mulay, L. N. Eds.; John Wiley and Sons: New York, 1976,

(42) (a) Hohenberg, P.; Kohn, W. *Phys. Rev*. **1964**, *136*, B864. (b) *Density-Functional Theory of Atoms and Molecules*, Parr, R. G.; Yang, W. Oxford University Press: Oxford, 1989.

(43) (a) Becke, A. D. *Phys. Rev. A***1988**, *38*, 3098. (b) Becke, A. D. *J. Chem. Phys.***1993**, *98*, 1372. (c) Becke, A. D. *J. Chem. Phys.***1993**, *98*, 5648.

(44) Lee, C. T.; Yang, W. T.; Parr, R. G. *Phys. Rev. B***1998**, *37*, 785.

(45) Frisch, M. J.; Trucks, G. W.; Schlegel, H. B.; Scuseria, G. E.; Robb, M. A.; Cheeseman, J. R.; Montgomery, J. A., Jr.; Vreven, T.; Kudin, K. N.; Burant, J. C.; Millam, J. M.; Iyengar, S. S.; Tomasi, J.; Barone,V.; Mennucci,B.; Cossi,M.; Scalmani,G.; Rega,N.; Petersson,G. A.; Nakatsuji, H.; Hada, M.; Ehara, M.; Toyota, K.; Fukuda, R.; Hasegawa, J.; Ishida, M.; Nakajima, T.; Honda, Y.;Kitao, O.;Nakai, H.; Klene, M.; Li, X.; Knox, J. E.; Hratchian, H. P.; Cross, J. B.; Adamo, C.; Jaramillo, J.; Gomperts, R.; Stratmann, R. E.; Yazyev, O.; Austin, A. J.; Cammi, R.; Pomelli, C.; Ochterski, J. W.; Ayala, P. Y.; Morokuma, V; Voth, G. A.; Salvador, P.; Dannenberg, J. J.; Zakrzewski, V. G.; Dapprich, S.; Daniels, A. D.; Strain, M. C.; Farkas, O.; Malick, D. K.; Rabuck, A. D.; Raghavachari, K.; Foresman, J. B.; Ortiz, J. V.; Cui, Q.; Baboul, A. G.; Clifford, S.; Cioslowski, J.; Stefanov, B. B.; Liu, G.; Liashenko, A.; Piskorz, P.; Komaromi, I.; Martin, R. L.; Fox, D. J.; Keith, T.; Al-Laham, M. A.; Peng, C. Y.; Nanayakkara, A.;

Challacombe, M.; Gill, P. M. W.; Johnson, B.; Chen, W.; Wong, M. W.; Gonzalez, C.; Pople, J. A. *Gaussian 03,* revision B.05; Gaussian, Inc.: Wallingford, CT, 2003.

(46) Dunning, T. H.; Hay, P. J. In *Modern Theoretical Chemistry*. *3. Methods of Electronic Structure Theory*; Schaefer, III, H. F. Ed.; Plenum Press: New York, 1977; pp 1−28.

(47) (a) Wadt, W. R.; Hay, P. J. *J. Chem. Phys.* **1985**, *82*, 284.(b) Wadt, W. R.; Hay, P. J. *J. Chem. Phys.***1985**, *82*, 299.

(48) Couty, M.; Hall, M. B. *J. Comput. Chem.* **1996,** *17*, 1359

(49) *SMART for Windows NT*, version 5.618; Bruker Advanced X-ray Solutions, Inc.: Madison, WI, 2001.

(50) *SAINT. Data Reduction Software. Version 6.36A*; Bruker Advanced X-ray Solutions, Inc.: Madison, WI, 2001.

(51) *SADABS. Area Detector Absorption and other Corrections Software, Version 2.05*; Bruker Advanced X-ray Solutions, Inc.: Madison, WI, 2001.

(52) Sheldrick, G. M. *SHELXTL, version 6.12*; Bruker Advanced X-ray Solutions, Inc.: Madison, WI, 2002.

(53) Marsh, R. E. *Acta Crystallogr*. **2009**, *B65*, 782

(54) Cotton F. A. *Q. Rev. Chem. Soc.* **1966**, *20*, 389

(55) Aguirre, J. D.; Chifotides, H. T.; Angeles-Boza, A. M.; Chouai, A.; Turro, C.; Dunbar, K. R. *Inorg. Chem.* **2009**, *48*, 4435

(56) Wade, C. R.; Dincă, M. *Dalton Trans.* **2012**, *41*, 7931

(57) Long, A. K. M.; Timmer, G. H.; Pap, J. S.; Snyder, J. L.; Yu, R. P.; Berry, J. F. *J. Am. Chem. Soc.* **2011**, *133*, 13138.

(58) Cotton, F. A.; in: F.A. Cotton, C.A. Murillo, R.A. Walton (Eds.), *Mult. Bonds Met. At.*, Springer US, **2005**: pp. 35.

(59) Cotton, F. A.; in: F.A. Cotton, C.A. Murillo, R.A. Walton (Eds.), *Mult. Bonds Met. At.*, Springer US, **2005**: pp. 69.

(60) Cotton, F. A.; Daniels, L. M.; Murillo, C. A.; Slaton, J. G. *J. Am. Chem. Soc*. **2002,** *124*, 2878.

(61) R.R. Schrock, L.G. Sturgeoff, P.R. Sharp, Inorg. Chem. 22 (1983) 2801. doi:10.1021/ic00162a008.

(62) Eglin, J. L. in: F.A. Cotton, C.A. Murillo, R.A. Walton (Eds.), *Mult. Bonds Met. At.*, Springer US, **2005**: pp. 183–202.

(63) Bailey, P. J.; Pace, S. *Chem. Rev.* **2001,** *21*, 491.

(64) Clérac, R.; Cotton, F. A.; Daniels, L. M.; Donahue, J. P.; Murillo, C. A.; Timmons, D. J. *Inorg. Chem.* **2000,** *39*, 2581

(65) Cotton, F. A.; Daniels, L. M.; Murillo, C. A.; Timmons, D. J.; Wilkinson, C.C. *J. Am. Chem. Soc.* **2002,** *124*, 9249

(66) Bailey, P. J.; Bone, S. F.; Mitchell, L. A.; Parsons, S.; Taylor, K. J.; Yellowlees, L. J. *Inorg. Chem.* **1997,** *36*, 867

(67) Cotton, F. A.; Dalal, N. S.; Hillard, E. A.; Huang, P.; Murillo, C. A.; Ramsey, C. M. *Inorg. Chem.* **2003,** *42*, 1388

(68) Pap, J. S.; Snyder, J. L.; Piccoli, P. M. B.; Berry, J. F. *Inorg. Chem.* **2009,** *48,* 9846.

(69) Berry, J. F.; Bothe, E.; Cotton, F. A.; Ibragimov, S. A.; Murillo, C. A.; Villagrán, D. et al., *Inorg. Chem.* **2006,** *45,* 4396

(70) Cotton, F. A.; Gruhn, N. E.; Gu, J.; Huang, P.; Lichtenberger, D. L.; Murillo, C. A. et al., *Science*. **2002,** *29,*81971

(71) Chiarella, G. M.; Cotton, F. A.; Durivage, J. C.; Lichtenberger, D. L.; Murillo, C. A. *J. Am. Chem. Soc.* **2013,** *135,* 17889

(72) Cotton, F. A.; Z. Li, C.A. Murillo, Inorg. Chem. 48 (2009) 11847. doi:10.1021/ic9018647.

(73) Cotton, F. A.; Murillo, C. A.; Young, M. D.; Yu, R.; Zhao, Q. *Inorg. Chem.* **2008,** *47*, 219

(74) Cotton, F. A.; Li, Z.; Liu, C. Y.; Murillo, C. A. *Inorg. Chem.* **2007,** *46,* 9294

(75) Cotton, F. A.; Li, Z.; Liu, C. Y.; Murillo, C. A. *Inorg. Chem.* **2007,** *46,*7840.

(76) Cotton, F. A.; Liu, C. Y.; Murillo, C. A.; Zhao, Q. *Inorg. Chem.* **2007,** *46,* 2604

(77) Cotton, F. A.; Li, Z.; Murillo, C. A.; Wang, X.; Yu, R.; Zhao, Q. *Inorg. Chem*. **2007,** *46,* 3245

(78) Cotton, F. A.; Murillo, C. A.; Zhao, Q. *Inorg. Chem*. **2007,** *46,* 6858

(79) Cotton, F. A.; Liu, C. Y.; Murillo, C. A.; Wang, X. *Inorg. Chem.* **2006,** *45,* 2619

(80) Cotton, F. A.; Liu, C. Y.; Murillo, C. A.; Zhao, Q. *Inorg. Chem.* **2006,** *45,* 9480.

(81) Chisholm, M. H.; Lear, B. J.; Moscatelli, A.; Peteanu, L. A. *Inorg. Chem.* **2010,** *49,*3706

(82) Barybin, M. V.; Chisholm, M. H.; Dalal, N.S.; Holovics, T.H.; Patmore, N. J.; Robinson, R. E. et al., *J. Am. Chem. Soc.* **2005,** *127,* 15182.

(83) Manke, D.R.; Loh ,Z.-H.; Nocera, D. G. *Inorg. Chem.* **2004,** *43*, 3618.

(84) Chisholm, M. H.; Hollandsworth, C. B.; in: F.A. Cotton, C.A. Murillo, R.A. Walton (Eds.), *Mult. Bonds Met. At.*, Springer US, **2005**: pp. 203

(85) Chiarella, G. M.; Cotton, F. A.; Murillo, C. A.; Zhao, Q. *Inorg. Chem*. **2014,** *53,* 2288.

(86) Gilbert, T. M.; Littrell, J. C.; Talley, C. E.; Vance, M. A.; Dallinger, R. F.; Rogers, R. D. *Inorg. Chem*. **2004,** *43,*1762.

(87) Cotton, F. A. in: F.A. Cotton, C.A. Murillo, R.A. Walton (Eds.), *Mult. Bonds Met. At.*, Springer US, **2005**: pp. 707

(88) Bursten, B. E.; Chisholm, M. H.; Clark, R. J. H.; Firth, S.; Hadad, C. M.; MacIntosh, A. M.; *J. Am. Chem. Soc.* **2002,** *124*, 3050–3063

(89) Cotton, F. A.; Li, Z.; Liu, C. Y.; Murillo, C. A.; Villagrán, D. *Inorg. Chem.* **2006,** *45,*767

Vita

Karen Ventura was born in El Paso, Texas. After completing her coursework at Instituto Tecnológico de Estudios Superiores de Monterrey in Cd. Juárez, México in 2009, Karen entered The University of Texas at El Paso. During the summer of 2011 she attended Versalius College in Brussels, Belgium. Later in the summer of 2012 she attended Shantou University in Shantou, China. She received a Bachelor of Science with a major in Chemistry in December 2012. In August 2013 she entered the Graduate School of The University of Texas at El Paso.